2D lattice material architectures for actuation

Nelissen, W.E.D.; Ayas, C.; Tekõglu, C.

Important note
To cite this publication, please use the final published version (if applicable).
Please check the document version above.

2D Lattice Material Architectures for Actuation

W. E. D. Nelissen[a], C. Ayas[a], C. Tekoğlu[b,*]

[a]*Structural Optimization and Mechanics Group, Department of Precision and Microsystems Engineering,*
Faculty of Mechanical, Maritime and Material Engineering, Delft University of Technology, Mekelweg 2, 2628 CD, Delft,
The Netherlands
[b]*Department of Mechanical Engineering, TOBB University of Economics and Technology, Söğütözü, Ankara, 06560, Turkey*

Abstract

The Kagome structure has been shown to be a highly suited micro-architecture for adaptive lattice materials, in which selected lattice members are replaced by actuators aiming to create shape morphing structures. It is the combination of in-plane isotropy, high stiffness and low energy requirement for actuation that makes the planar Kagome structure the best performing micro-architecture known to date. Recently, Pronk et al. (2017) have proposed a set of topological criteria to identify other micro-architectures suitable for actuation. In the present paper, four novel lattice topologies are presented which were contrived in light of these criteria. Matrix analysis is performed to reveal the static and kinematic properties of the pin-jointed versions of these four structures. The finite element method is used to determine their stiffness and actuation characteristics. One of the proposed designs is found to match the optimal elastic properties of the Kagome structure, while it requires less energy for (single member) actuation. However, the displacement field induced by actuation attenuates faster than in a Kagome lattice. The presented results also show that the criteria proposed by Pronk et al. (2017) should be refined in two regards: *i)* statically indeterminate lattice materials do not necessarily result in high actuation energy and thus should not be ruled out, and *ii)* as shown by counterexample, the criteria are not sufficient.

Keywords: Cellular solids, Lattice Materials, Static/kinematic determinacy, Shape morphing, Actuators, Finite element method

1. Introduction

Lattice materials are a type of cellular solids comprising many slender lattice members (rods or beams), and are characterised by a repetitive structure. Each cell in a lattice material has exactly the same shape and dimensions, and the slender members —also referred to as struts— meet on lattice points. This is in contrast to other cellular solids. For example, open-cell foams comprise members having a range of dimensions and a random micro-architecture. Consequently, the representative volume element of a foam is relatively large. The repetitive micro-architecture of a lattice material, on the other hand, can be described by a small periodic unit cell with only a few struts. In planar (2D) lattice materials, a polygonal unit cell tessellates the plane, while in spatial (3D) lattice materials, the space is tessellated by a polyhedron.

The term *lattice material* is used to emphasise that the lattice behaves like a *material*, i.e. it can be treated as a homogenised continuum with macroscopic properties such as elastic moduli and yield strength (e.g. Onck (2002); Wang and McDowell (2004)). This is justified when both the global length scale of the lattice and the wavelength(s) of loading are much larger than the dimensions of the unit cell. Lattices that do not comply with these requirements behave like a structure and hence are not classified as lattice materials. The macroscopic properties of a lattice material are dictated by three factors: material properties of the

---

*Corresponding author. Tel.:+90 312 292 42 29 ; fax:+90 312 292 40 91.
Email address: cihantekoglu@etu.edu.tr; C.Tekoglu@gmail.com (C. Tekoğlu)

strut material, relative density $\bar{\rho}$ (volume fraction of struts), and the micro-architecture (Ashby et al., 2000). The effects of the first two factors on the material properties are limited in comparison to that of the lattice micro-architecture, which offers the key design freedom to control the macroscopic mechanical properties.

Lattice materials have drawn attention in the context of shape morphing/adaptive materials. Shape morphing structures can be constructed by replacing selected members of a lattice by actuators, which have the ability to lengthen or shorten in response to an external stimulus. Length changes of these actuators cause deformations in the lattice; see e.g. Donev and Torquato (2003), Hutchinson et al. (2003) and Wicks and Guest (2004).

Depending on the micro-architecture, the actuation energies of lattice materials differ by orders of magnitude. Moreover, the extent to which actuation-induced deformations spread varies greatly between micro-architectures. Structures that require a small amount of energy for actuation, while the deformations spread over a large region are of interest, because such structures are capable of effective macroscopic shape change.

Planar adaptive lattice materials can be used to construct 3D shape morphing structures. For example, a sandwich panel can be constructed featuring an adaptive planar lattice as one or both of its face sheets, and a core comprising a foam or a regular 3D lattice. Depending on the adaptive lattice micro-architecture and placement of the actuators, both in- and out-of-plane deformations of the sandwich structure can be achieved; see e.g. Hutchinson et al. (2003), Wicks and Hutchinson (2004), dos Santos e Lucato et al. (2004) and dos Santos e Lucato et al. (2005).

The ideal lattice material for actuation features high macroscopic elastic moduli and strength. Isotropic elasticity is desirable in order for the lattice material to exhibit these mechanical properties irrespective of the loading direction. Finally, the lattice material should be compliant in response to actuation when selected members are replaced by actuators. Simultaneous fulfilment of these requirements is rare, as micro-architectures with high stiffness generally show large resistance to actuation-driven deformation. This does not rule out all lattice materials from being suitable for actuation, but requires a careful investigation of the elastic deformation characteristics of different lattices.

Two distinct types of elastic deformation are encountered when lattice materials are subjected to external loads [1]. That is, the deformation of a lattice is dominated by either stretching or bending of its members. The former results in much higher macroscopic elastic moduli, since the axial stiffness of slender struts is much higher than their bending stiffness. Whether a lattice micro-architecture is stretching- or bending-dominated can be determined from the kinematic properties of the equivalent pin-jointed truss. If that repetitive pin-jointed truss does not have any inextensional mode of deformation (mechanism) that can be excited by a uniform macroscopic strain state, the corresponding rigid-jointed lattice material is stretching-dominated. Conversely, the presence of one or more of such mechanisms for the repetitive pin-jointed truss results in bending-dominated deformation of the equivalent rigid-jointed lattice. Macroscopic elastic moduli of a stretching-dominated lattice material scale approximately linearly with relative density $\bar{\rho}$, whereas for a bending-dominated 2D lattice material, the macroscopic elastic moduli scale with $\bar{\rho}^3$ (Gibson and Ashby, 1997; Deshpande et al., 2001; Wang and McDowell, 2004; Fleck, 2004).

The resistance of a lattice material to actuation also depends on its micro-architecture and can be quantified by the amount of strain energy that is stored after actuating a single member in a large lattice. Wicks and Guest (2004) investigated single member actuation of three lattices with different topologies by means of calculating actuation energy through finite element (FE) analysis. The study revealed that the fully triangulated lattice, with no mechanisms when pin-jointed, consumes significantly more energy than the bending-dominated hexagonal lattice. The pin-jointed hexagonal truss does possess mechanisms that can be excited by a uniform macroscopic strain state. The third structure investigated by Wicks and Guest (2004) is the Kagome lattice, which is currently unmatched in its performance as an adaptive lattice material. Although the pin-jointed Kagome truss has a mechanism, the rigid-jointed Kagome lattice shows stretching-dominated deformation behaviour. Its specific elastic properties are equal to those of the fully triangulated lattice (Hyun and Torquato, 2002; Wang and McDowell, 2004), which are optimal for an isotropic 2D cellular solid. Conversely, the energy required for actuation of the Kagome lattice is considerably less compared to the fully triangulated lattice, (for the same bar stockiness).

---

[1]Only uniform macroscopic loading states are considered in this paper and rotation gradients are ignored.

The kinematic and static properties of the pin-jointed repetitive Kagome truss were investigated by Guest and Hutchinson (2003). This study concluded that no infinite (repetitive) truss can be simultaneously kinematically and statically determinate, unlike finite trusses. Moreover, it was found that the static determinacy of a repetitive truss in 2D requires the truss to possess 3 states of self-stress such that it can sustain any state of planar macroscopic stress. Recently, Pronk et al. (2017) proposed that, for a repetitive lattice material to be suitable for actuation, its pin-jointed version should be statically determinate and satisfy Maxwell's stability criterion (Maxwell, 1864; Pellegrino and Calladine, 1986). A direct consequence of that for the repetitive truss is to have one mechanism. Pronk et al. (2017) also showed that the existence of such a mechanism is not detrimental to the macroscopic stiffness of the rigid-jointed lattice material, granted it is a *non strain-producing* mechanism, i.e. it cannot be excited by a macroscopic strain state.

Inspired by the Kagome lattice and its unique properties, this paper continues the quest for 2D lattice designs that can compete with the Kagome micro-architecture. Four candidate structures were contrived in light of the criteria proposed by Pronk et al. (2017). Section 2 summarises the most important results of Pronk et al. (2017) and explains the selection of the micro-architectures to be studied. In section 3, static and kinematic properties of the pin-jointed repetitive trusses are analysed using the matrix method of Pellegrino and Calladine (1986). Section 4 details how the macroscopic elastic properties of the rigidly jointed lattices are determined using the FE method, followed by Section 5 in which FE calculations that quantify the actuation performance of all the lattices are presented. The results of the different analyses are discussed in Section 6. Section 7 summarises the most salient points of the paper.

2. Preselection

The mechanical properties of a lattice material with rigidly connected struts are closely related to the rigidity of its pin-jointed counterpart. Therefore, the concepts of statical and kinematical determinacy, which are central in determining the rigidity of a pin-jointed truss are also key to identifying stretching-dominated lattice materials with high stiffness.

First, consider a finite truss with no foundational supports. Such a truss can be both statically and kinematically determinate, i.e. *just rigid*, if the number of bars b is equal to the total number of degrees of freedom nj where $n = 2$ for a two-dimensional (2D) truss and $n = 3$ in case of a three-dimensional (3D) truss, and j is the total number of joints. However, simultaneous static and kinematic determinacy is acquired only if the bars are properly positioned. In other words, the Maxwell condition $b = nj$ is a necessary but not sufficient criterion for a finite truss to be *just rigid*.

Recall that lattice materials by definition consist of a large number of unit cells. Therefore, it is appropriate to consider the rigidity of the equivalent repetitive pin-jointed truss for an indication of the mechanical performance of a lattice material. While a repetitive truss is infinitely large, it can be represented by a periodic unit cell where loads and deformations are assumed to repeat with the repetition of this unit cell through n-dimensional space. Equilibrium equations can then be set up, relating the forces acting on the joints to the tensions arising in the bars of the unit cell. In matrix form, the $nj \times b$ equilibrium matrix $\mathbf{A}$, post-multiplied with the $b \times 1$ vector of bar tensions[2] $\mathbf{t}$ yields the $nj \times 1$ nodal force vector $\mathbf{f}$, i.e.

$$\mathbf{At} = \mathbf{f}. \tag{1}$$

For a 2D repetitive truss to be rigid, it must be able to sustain any combination of the three possible remote loadings at infinity (σ_{11}, σ_{22} and σ_{12}) with zero nodal forces ($\mathbf{f} = \mathbf{0}$) (Guest and Hutchinson, 2003). This implies that $\mathbf{A}$ must be rank-deficient by *at least* three; the truss must have three or more states of self-stress, which are represented by the columns of the nullspace of $\mathbf{A}$. Using the method of sections, (linear combinations of) these states of self-stress must evaluate to the three possible macroscopic stresses in 2D (Hutchinson and Fleck, 2006).

---

[2]It is convenient to use a tension coefficient, defined as tension per member length, instead of the tension for each bar. Then the corresponding measure of elongation of the bar is an elongation coefficient, defined as elongation times member length. We shall use the terms tension, elongation in the remainder to refer to these convenient parameters.

A kinematic assessment of a 2D repetitive truss leads to a another system of equations that can be cast into matrix form as

$$\mathbf{Bd} = \mathbf{e}, \tag{2}$$

where $\mathbf{d}$ is the $nj \times 1$ nodal displacement vector and $\mathbf{e}$ is the $b \times 1$ bar elongation vector. $\mathbf{B}$ is the $b \times nj$ compatibility matrix and $\mathbf{A}^{\mathrm{T}} = \mathbf{B}$ by virtue of the principle of virtual work. Consequently, the rank of $\mathbf{B}$ is equal to the rank of $\mathbf{A}$. The nullspace of $\mathbf{B}$ contains inextensional displacement modes: non-zero displacement vectors that satisfy Eq. (2) for $\mathbf{e} = \mathbf{0}$. In case of a repetitive truss, such a displacement mode is either a rigid-body translation or a mechanism. Rigid-body rotation is impossible as it violates the periodicity conditions.

Mechanisms of a repetitive truss can be classified into infinitesimal and finite mechanisms. For finite mechanisms, joints can displace by finite amounts while the length of each member of the truss is preserved. An infinitesimal mechanism, on the other hand, leads to small (of second or higher order in terms of joint displacements) changes in one or more members' lengths. Consequently, infinitesimal mechanisms tighten up after infinitesimally small displacements of joints. A key assumption in matrix analysis is that the displacements of joints are sufficiently small so that the equilibrium/compatibility equations for the reference (undeformed) configuration remain accurate. That is, the static/kinematic equations are linearised in the undeformed configuration. The linearised mechanisms found through matrix analysis therefore represent mechanisms that in reality are either infinitesimal or finite. The analysis cannot distinguish between the two.

Mechanisms can be also classified into two subgroups depending on whether they are strain-producing or not. The key characteristic of a non strain-producing mechanism is that its linearised version does not induce any macroscopic strain. Vice versa, such a mechanism is not excited when the repetitive structure endures macroscopic strain.

Static and kinematic determinacy for infinite repetitive trusses are not universally defined. Here, the definitions of Guest and Hutchinson (2003) are adopted: a 2D repetitive structure is statically determinate if there are exactly three non-zero solutions to the equilibrium equations $\mathbf{At} = \mathbf{0}$ that correspond to the three possible stress states in 2D. A kinematically determinate 2D repetitive truss is one where the only solutions to the compatibility equations $\mathbf{Bd} = \mathbf{0}$ are the two rigid body translations, ruling out the existence of a mechanism. That is, static determinacy requires $\mathbf{A}$ to be rank-deficient by three, while kinematic determinacy requires $\mathbf{B}$ to be rank-deficient by two; since $\mathbf{A}^{\mathrm{T}} = \mathbf{B}$, an infinite repetitive truss cannot be both statically and kinematically determinate.

The simultaneous requirement of high stiffness and low-energy actuation is the main challenge in the search for an ideal adaptive lattice micro-architecture. That is, the rigidly jointed lattice material must deform in a stretching-dominated manner in response to macroscopic loads. Nevertheless, when one or more bars are replaced with an actuator, a length change of the actuator(s) should cause the remaining lattice material to deform compliantly; actuation should induce bending-dominated deformation. After thorough analysis of a number of lattice micro-architectures, Pronk et al. (2017) proposed that for an isotropic 2D lattice material to be suitable for actuation, its pin-jointed version:

   i) must satisfy Maxwell's stability criterion,
   ii) must be statically determinate and
   iii) must have one *non strain-producing* mechanism only.

In generalised form, Maxwell's rule reads

$$s - m = b - 2j = 0, \tag{3}$$

in the absence of foundational constraints. The number of states of self-stress is represented by s, while m is the number of inextensional displacement modes. If a repetitive pin-jointed structure is also statically determinate, $s = m = 3$, leaving the structure with one mechanism in addition to the two rigid-body translations. The third criterion proposed by Pronk et al. (2017) concerns the mechanism of a statically determinate truss. The appearing mechanism must be *non strain-producing*. If so, the periodic truss is rigid and the equivalent lattice material is stiff owing to a stretching-dominated deformation response to macroscopic loads. On the other hand, a member replaced by an actuator may excite a mechanism for
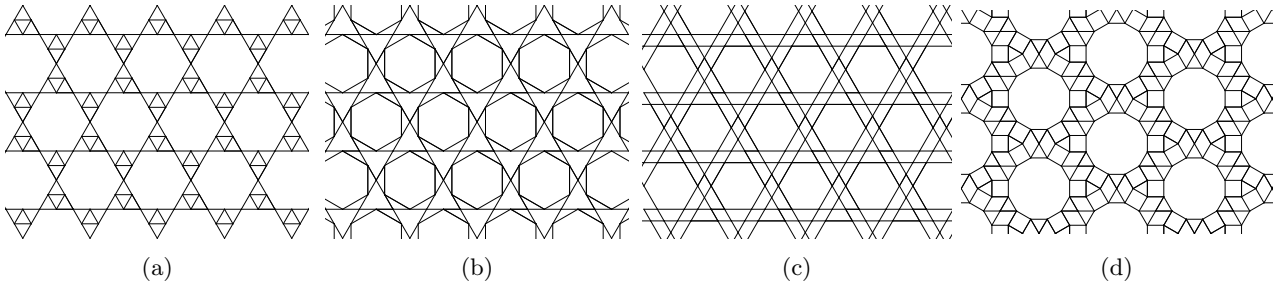
Figure 1: Lattice micro-architectures investigated: (a) Kagome with concentric triangles (KT), (b) Kagome with concentric hexagons (KH), (c) Double Kagome (DK) and (d) the Modified Dodecagonal structure (MD).

the truss, causing the equivalent lattice material to deform in a bending-dominated fashion. Such a lattice material would therefore require low energy for actuation. In fact, the rigidity of a repetitive truss with the ideal micro-architecture is reminiscent of the rigidity of a finite truss that is *just rigid*. The Kagome structure is the only micro-architecture among the regular and semi-regular tessellations of the plane that satisfies these criteria (Pronk et al., 2017).

The four lattice micro-architectures that are investigated in this paper are shown in Fig. 1. These designs have not been investigated in previous literature, to the best of our knowledge. The first three micro-architectures, displayed in Figs. 1a–c are closely related to the Kagome lattice. The **K**agome with concentric **T**riangles (KT) structure is attained by dissecting each triangle in a Kagome lattice into four equilateral triangles of equal size; see Fig. 1a. Similarly, the **K**agome with concentric **H**exagons (KH) features an additional concentric hexagon within each hexagon that is present in a regular Kagome lattice; see Fig. 1b. The **D**ouble **K**agome (DK) structure is shown in Fig. 1c. For each (infinitely long) line appearing in the Kagome structure, the DK structure shows two parallel sets of aligned members. The fourth micro-architecture considered is the **M**odified **D**odecagonal structure (MD), depicted in Figure 1d. It is based on the 2-uniform '3-4-6-12 tiling' (Critchlow, 1970). Dodecagons are the largest polygons appearing in the 3-4-6-12 tiling. The MD structure is constructed by dissecting all of the hexagons in the 2-uniform tiling into two equilateral triangles and two rhombi. This is done such that the six-fold rotational symmetry is preserved. The MD and Hexagonal Cupola micro-architectures are closely related. Pronk et al. (2017) have investigated the latter and concluded that it is not suitable for actuation purposes because of its bending-dominated deformation behaviour. The MD structure is expected to have more favourable mechanical properties. The reason for this is the fact that there are no uninterrupted (infinite) arrays of parallel members in this structure, which there are in each of the Hexagonal, Hexagonal Cupola, and 3-4-6-12 architectures. The KT and MD micro-architectures, depicted in Fig. 1a and d, respectively, have a uniform member length, whereas the KH and DK micro-architecture shown in Fig. 1b and c, feature members of two different lengths.

Note that all four lattices shown in Fig. 1 are in-plane isotropic owing to the three-fold rotational symmetry; see e.g. Ayas and Tekoğlu (2018). Furthermore, all four micro-architectures have a valency of four, giving $b = 2j$ in Eq. (3). Consequently, the structures fulfil the first of the proposed criteria by Pronk et al. (2017), and thus have square equilibrium and compatibility matrices.

3. Static and kinematic properties of the preselected pin-jointed lattices

It remains to study the kinematic and static properties of the repetitive trusses with the preselected micro-architectures in order to determine whether the second and third criteria proposed by Pronk et al. (2017) are also fulfilled. For that purpose, matrix analysis (Pellegrino and Calladine, 1986) is performed on representative periodic unit cells, illustrated in Fig. 2. First, statics is considered and states of self-stress of each of the structures are identified. Next, kinematics is considered and inextensional displacement modes are identified. For the sake of brevity, a detailed description of the matrix analyses are given for the KT structure only, whereas for other micro-architectures, results are reported and compared only.

5
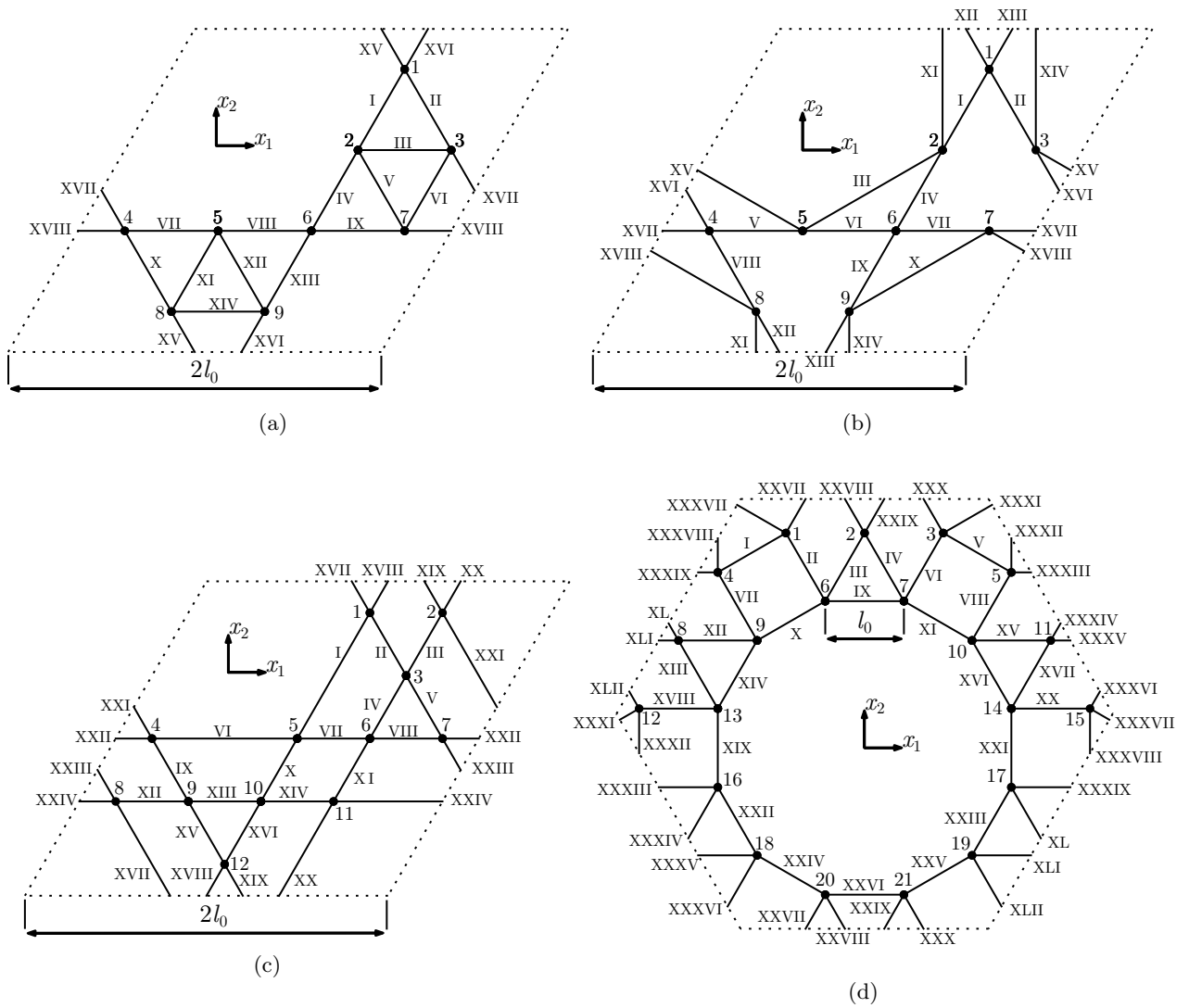
Figure 2: Selected unit cells for matrix analysis of repetitive pin-jointed trusses with the proposed micro-architectures: (a) KT, (b) KH, (c) DK and (d) MD. Nodes are labelled with Hindu-Arabic numerals, struts are indicated with Roman numerals. A reference length l_0 is defined in each of the unit cells.

3.1. States of Self-stress

Matrix analysis of a repetitive truss concerns forces on nodes and tensions arising in members within a chosen unit cell. The KT unit cell depicted in Fig. 2a contains nine nodes numbered with Hindu-Arabic numerals and eighteen members numbered with Roman numerals. Coordinate systems are also indicated in Fig. 2. All nodes are situated in the interior of the unit cell. Members that cross a unit cell boundary, such as member XV, are effectively connected to two nodes of the (same) unit cell. A total of 18 independent nodal forces are stored in the vector $\mathbf{f} = [f_1^{(1)} \ f_2^{(1)} \ ... \ f_1^{(9)} \ f_2^{(9)}]^{\mathrm{T}}$, where $f_i^{(J)}$ denotes the force in the x_i-direction acting on node J. A total of 18 bar tension comprise the bar tension vector $\mathbf{t} = [t^{\mathrm{I}} \ t^{\mathrm{II}} ... \ t^{\mathrm{XVIII}}]^{\mathrm{T}}$. Following Eq. (1), $\mathbf{t}$ is directly related to the nodal force vector $\mathbf{f}$ through the 18×18 equilibrium matrix $\mathbf{A}$. The entries of the equilibrium matrix are determined from the unit cell micro-architecture. The equilibrium matrix for the repetitive KT truss reads

$$
\mathbf{A} = \begin{bmatrix}
\frac{1}{2} & -\frac{1}{2} & 0 & 0 & 0 & 0 & 0 & 0 & 0 & 0 & 0 & 0 & 0 & 0 & \frac{1}{2} & -\frac{1}{2} & 0 & 0 \\
\frac{\sqrt{3}}{2} & \frac{\sqrt{3}}{2} & 0 & 0 & 0 & 0 & 0 & 0 & 0 & 0 & 0 & 0 & 0 & 0 & -\frac{\sqrt{3}}{2} & -\frac{\sqrt{3}}{2} & 0 & 0 \\
-\frac{1}{2} & 0 & -1 & \frac{1}{2} & -\frac{1}{2} & 0 & 0 & 0 & 0 & 0 & 0 & 0 & 0 & 0 & 0 & 0 & 0 & 0 \\
-\frac{\sqrt{3}}{2} & 0 & 0 & \frac{\sqrt{3}}{2} & \frac{\sqrt{3}}{2} & 0 & 0 & 0 & 0 & 0 & 0 & 0 & 0 & 0 & 0 & 0 & 0 & 0 \\
0 & \frac{1}{2} & 1 & 0 & 0 & \frac{1}{2} & 0 & 0 & 0 & 0 & 0 & 0 & 0 & 0 & 0 & 0 & -\frac{1}{2} & 0 \\
0 & -\frac{\sqrt{3}}{2} & 0 & 0 & 0 & \frac{\sqrt{3}}{2} & 0 & 0 & 0 & 0 & 0 & 0 & 0 & 0 & 0 & 0 & \frac{\sqrt{3}}{2} & 0 \\
0 & 0 & 0 & 0 & 0 & 0 & -1 & 0 & 0 & -\frac{1}{2} & 0 & 0 & 0 & 0 & 0 & 0 & \frac{1}{2} & 1 \\
0 & 0 & 0 & 0 & 0 & 0 & 0 & 0 & 0 & \frac{\sqrt{3}}{2} & 0 & 0 & 0 & 0 & 0 & 0 & -\frac{\sqrt{3}}{2} & 0 \\
0 & 0 & 0 & 0 & 0 & 0 & 1 & -1 & 0 & 0 & \frac{1}{2} & -\frac{1}{2} & 0 & 0 & 0 & 0 & 0 & 0 \\
0 & 0 & 0 & 0 & 0 & 0 & 0 & 0 & 0 & 0 & \frac{\sqrt{3}}{2} & \frac{\sqrt{3}}{2} & 0 & 0 & 0 & 0 & 0 & 0 \\
0 & 0 & 0 & -\frac{1}{2} & 0 & 0 & 0 & 1 & -1 & 0 & 0 & 0 & \frac{1}{2} & 0 & 0 & 0 & 0 & 0 \\
0 & 0 & 0 & -\frac{\sqrt{3}}{2} & 0 & 0 & 0 & 0 & 0 & 0 & 0 & 0 & \frac{\sqrt{3}}{2} & 0 & 0 & 0 & 0 & 0 \\
0 & 0 & 0 & 0 & \frac{1}{2} & -\frac{1}{2} & 0 & 0 & 1 & 0 & 0 & 0 & 0 & 0 & 0 & 0 & 0 & -1 \\
0 & 0 & 0 & 0 & -\frac{\sqrt{3}}{2} & -\frac{\sqrt{3}}{2} & 0 & 0 & 0 & 0 & 0 & 0 & 0 & 0 & 0 & 0 & 0 & 0 \\
0 & 0 & 0 & 0 & 0 & 0 & 0 & 0 & 0 & \frac{1}{2} & -\frac{1}{2} & 0 & 0 & -1 & -\frac{1}{2} & 0 & 0 & 0 \\
0 & 0 & 0 & 0 & 0 & 0 & 0 & 0 & 0 & -\frac{\sqrt{3}}{2} & -\frac{\sqrt{3}}{2} & 0 & 0 & 0 & \frac{\sqrt{3}}{2} & 0 & 0 & 0 \\
0 & 0 & 0 & 0 & 0 & 0 & 0 & 0 & 0 & 0 & 0 & \frac{1}{2} & -\frac{1}{2} & 1 & 0 & \frac{1}{2} & 0 & 0 \\
0 & 0 & 0 & 0 & 0 & 0 & 0 & 0 & 0 & 0 & 0 & -\frac{\sqrt{3}}{2} & -\frac{\sqrt{3}}{2} & 0 & 0 & \frac{\sqrt{3}}{2} & 0 & 0
\end{bmatrix}. \tag{4}
$$

The rank of this equilibrium matrix is 15, thus its nullspace contains $18 - 15 = 3$ linearly independent states of self-stress which are all possible combinations of bar tensions that are in equilibrium with zero nodal loads,

$$
\mathrm{null}(\mathbf{A}) = \begin{bmatrix}
1 & 0 & 0 & 1 & 0 & 0 & 0 & 0 & 0 & 0 & 0 & 0 & 1 & 0 & 0 & 1 & 0 & 0 \\
0 & 1 & 0 & 0 & 0 & 0 & 0 & 0 & 0 & 1 & 0 & 0 & 0 & 0 & 1 & 0 & 1 & 0 \\
0 & 0 & 0 & 0 & 0 & 0 & 1 & 1 & 1 & 0 & 0 & 0 & 0 & 0 & 0 & 0 & 0 & 1
\end{bmatrix}^{\mathrm{T}}. \tag{5}
$$

Each of these three states of self-stress is characterised by a set of aligned members sustaining the same tension. The first and second states of self-stress concern members that are rotated with respect to the x_1-axis by 60°, clockwise and anti-clockwise, respectively. They are illustrated in Figs. 3a and 3b. The third column vector in $\mathrm{null}(\mathbf{A})$ involves members that are oriented parallel to the x_1-direction, see Fig. 3c. The method of sections can be used to relate these states of self-stress (or their combinations) to average macroscopic stress states corresponding to loads at infinity. Let S denote the number of macroscopic stress states that a lattice is able to carry. In 2D, the maximum value of S is three. The 3D space of macroscopic stress states is then defined by three orthogonal base vectors that can be chosen as *i)* tension in the x_1-direction, *ii)* tension in the x_2-direction, and *iii)* shear loading in the $x_1 x_2$-plane, for example, can be chosen as the three orthogonal basis vectors for the space of macroscopic stress states. In fact, determining the state of macroscopic stress corresponding to a state of self-stress can be thought of as determining the projection of an 18 dimensional vector onto the 3D subspace of macroscopic stress states. By taking linear combinations of the vectors listed as columns of $\mathrm{null}(\mathbf{A})$ in Eq. (5), it is therefore possible to express the three states of self-stress for the KT
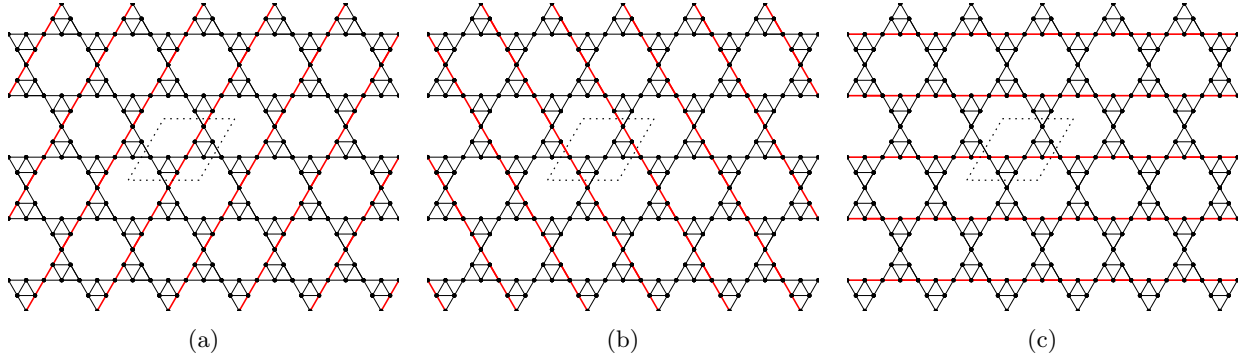
Figure 3: The three linearly independent states of self-stress of the KT micro-architecture. Members under tension are depicted bold and red. (a), (b), and (c) represent the first, second and third column of Null($\mathbf{A}$), respectively.
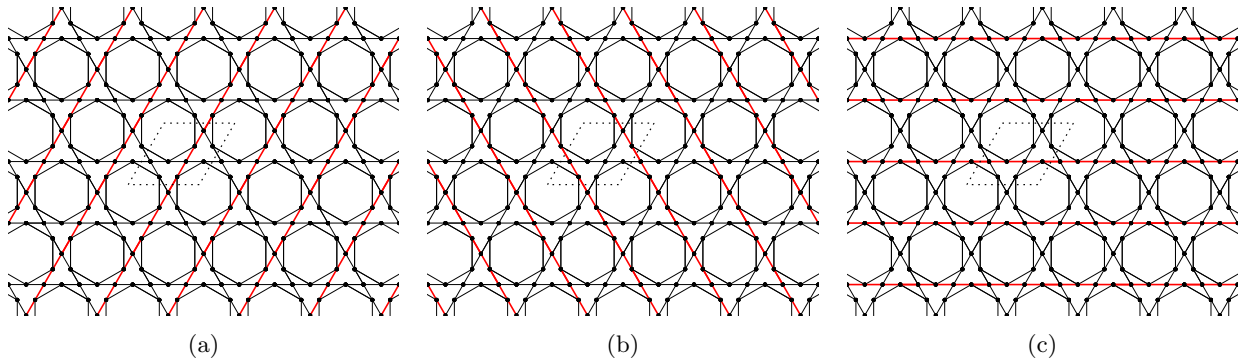
Figure 4: The three linearly independent states of self-stress of the KH micro-architecture. Members under tension are depicted bold and red. (a), (b), and (c) represent the first, second and third column of Null($\mathbf{A}$), respectively. Null($\mathbf{A}$) is given in Appendix.

structure with three new vectors. The projection of each of these vectors onto the subspace of macroscopic stress states coincides with an orthogonal axis:

Vector 1 = State 3 : $\quad \Sigma_{11} \neq 0, \quad \Sigma_{22} = \Sigma_{12} = 0.$

Vector 2 = State 1 + State 2 $- \frac{1}{2} \times$ State 3 : $\quad \Sigma_{22} \neq 0, \quad \Sigma_{11} = \Sigma_{12} = 0,$

Vector 3 = State 1 $-$ State 2 : $\quad \Sigma_{12} \neq 0, \quad \Sigma_{11} = \Sigma_{22} = 0,$

Clearly, the pin-jointed structure can support all three linearly independent states of macroscopic stress, i.e. $S = 3$.

The KH structure has very similar states of self-stress with $s = S = 3$; see Fig. 4. Thus, rigidly-jointed lattices with either of these architectures can sustain any macroscopic load without having members endure a significant bending load. Still, some members, namely those that form the 'internal' triangles in the KT and 'internal' hexagons in the KH structure, are stress-free in each of the states of self-stress shown in Figures 3 and 4. This suggests that, also in a rigidly-jointed KT or KH lattice material, these members will not contribute significantly to the macroscopic stiffness. Therefore, sub-optimal elastic properties are expected for lattice materials with either of these micro-architectures.

The DK structure has six linearly independent states of self-stress, see Fig. 5; $s = 6$ while $S = 3$. For this structure, the six states of self-stress can be expressed by an alternative set of six linearly independent vectors such that the projections onto the subspace of macroscopic stress states for the first three of these vectors coincide respectively with the three orthogonal axes, and for the remaining three the projections give zero vectors:

8
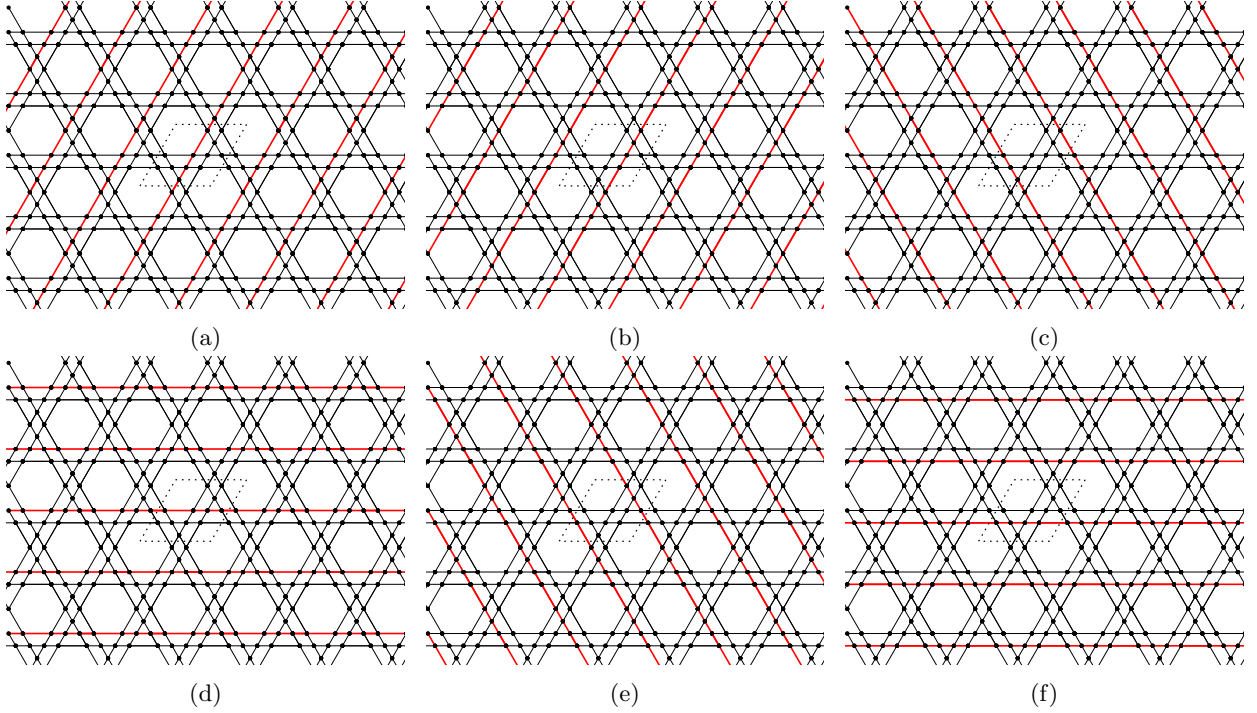
Figure 5: The six linearly independent states of self-stress of the Double Kagome micro-architecture; (a)–(f) represent column 1–6 of Null($\mathbf{A}$), respectively. The bar tension value is equal to 1 for the red members, and 0 for the black members. See Appendix for Null($\mathbf{A}$).

Vector 1 = State 4 + State 6 : $\Sigma_{11} \neq 0, \quad \Sigma_{22} = \Sigma_{12} = 0.$

Vector 2 = State 1 + State 2 + State 3 $- \frac{1}{2} \times$State 4 + State 5 $- \frac{1}{2} \times$State 6 : $\Sigma_{22} \neq 0, \quad \Sigma_{11} = \Sigma_{12} = 0,$

Vector 3 = State 1 + State 2 $-$ State 3 $-$ State 5: $\Sigma_{12} \neq 0, \quad \Sigma_{11} = \Sigma_{22} = 0,$

Vector 4 = State 1 $-$ State 2 : $\Sigma_{11} = \Sigma_{22} = \Sigma_{12} = 0,$

Vector 5 = State 3 $-$ State 5 : $\Sigma_{11} = \Sigma_{22} = \Sigma_{12} = 0,$

Vector 6 = State 4 $-$ State 6 : $\Sigma_{11} = \Sigma_{22} = \Sigma_{12} = 0.$

The states of self-stress corresponding to these six vectors are shown in Fig. 6, respectively.

Following the adopted definition, this structure is statically indeterminate, or redundant (overdeterminate). However, looking closer at the states of self-stress depicted in Fig. 5a-f, each of them involves a (different) set of aligned members, similar to the previous structures. In fact, upon summing all the stress states in Fig. 5a-f, not only are all members in the truss loaded, but the bar tensions are also equal. This indicates optimal use of material analogous to the Kagome micro-architecture. Therefore, DK lattice material is anticipated to have high macroscopic elastic moduli.

The MD structure is topologically unrelated to the other structures. It has $s = 4$ linearly independent states of self-stress which are visualised in Fig. 7. This implies that the MD structure too is statically indeterminate. The magnitude of the bar tension differs between members in all four states of self-stress. The varying levels of tension in the members will affect the the stiffness and strength of an equivalent lattice material with this micro-architecture. The most heavily stressed members will deform more and fail prior to others. Similar to the DK structure, the four states of self-stress for the MD structure can be expressed by an alternative set of four linearly independent vectors such that the projections onto the subspace of

9
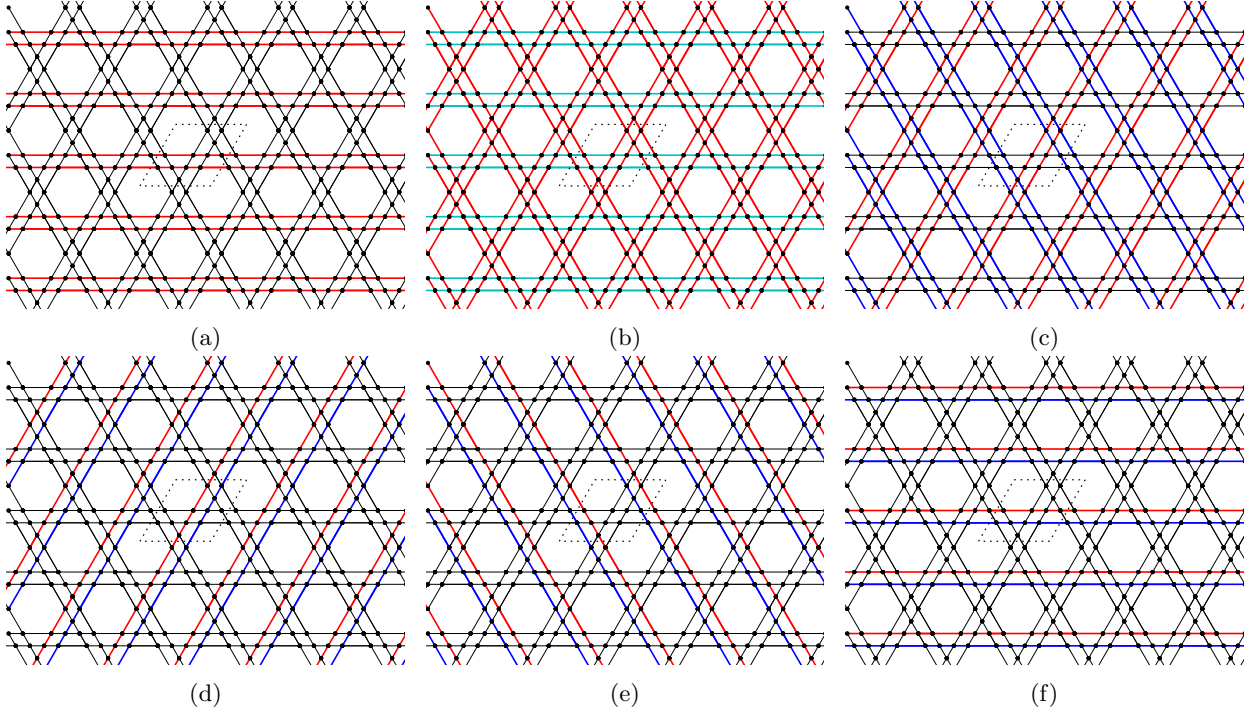
Figure 6: An alternative set of six linearly independent states of self-stress of the Double Kagome micro-architecture. The bar tension value is equal to 1 for the red members, -1 for the blue members, -1/2 for the green members, and 0 for the black members.

macroscopic stress states for the first three of these vectors coincide respectively with the three orthogonal axes, and for the fourth the projection gives zero vector:

Vector $1 = \frac{1}{2} \times$State $1 + \frac{1}{2} \times$State $2 + 2 \times$State $3 - 3 \times$State 4 : $\quad \Sigma_{11} \neq 0, \quad \Sigma_{22} = \Sigma_{12} = 0.$

Vector $2 =$ State $1 +$ State $2 - 2 \times$State 4 : $\quad \Sigma_{22} \neq 0, \quad \Sigma_{11} = \Sigma_{12} = 0,$

Vector $3 =$ State $1 -$ State 2 : $\quad \Sigma_{12} \neq 0, \quad \Sigma_{11} = \Sigma_{22} = 0,$

Vector $4 =$ State $1 +$ State $2 +$ State $3 - 2 \times$State 4 : $\quad \Sigma_{11} = \Sigma_{22} = \Sigma_{12} = 0.$

The states of self-stress corresponding to these four vectors are shown in Figs. 8, respectively.

3.2. Inextensional displacement modes

Since all the preselected micro-architectures are shown to yield rigid repetitive pin-jointed trusses with $S = 3$, the existence of a strain-producing mechanism in either of the micro-architectures is ruled out; the number of strain-producing mechanisms denoted by ms is zero. Consequently, the third criterion proposed by Pronk et al. (2017) is fulfilled by all the micro-architectures under consideration. The inextensional displacement modes are identified below for the sake of completeness.

Recall that a periodic pin-jointed truss with the KT architecture has a square equilibrium matrix $\mathbf{A}$. Therefore, its compatibility matrix $\mathbf{B} = \mathbf{A}^{\mathrm{T}}$ is also square. Following Eq. (2), the vector of member elongations $\mathbf{e} = [e^{\mathrm{I}} \; ... \; e^{\mathrm{XVIII}}]^{\mathrm{T}}$ is directly related to the nodal displacement vector $\mathbf{d} = [d_1^{(1)} \; d_2^{(1)} \; ... \; d_1^{(9)} \; d_2^{(9)}]^{\mathrm{T}}$ through the 18×18 compatibility matrix $\mathbf{B}$. The rank of this compatibility matrix is 15, indicating it has a nullspace containing $18 - 15 = 3$ linearly independent inextensional displacement modes:

$$\text{null}(\mathbf{B}) = \begin{bmatrix} 0 & 1 & 0 & 1 & 0 & 1 & 0 & 1 & 0 & 1 & 0 & 1 & 0 & 1 & 0 & 1 & 0 & 1 \\ 1 & 0 & 1 & 0 & 1 & 0 & 1 & 0 & 1 & 0 & 1 & 0 & 1 & 0 & 1 & 0 & 1 & 0 \\ \sqrt{3} & -1 & \frac{\sqrt{3}}{2} & -\frac{1}{2} & \frac{\sqrt{3}}{2} & -\frac{3}{2} & 0 & -2 & 0 & -1 & 0 & 0 & 0 & -1 & \frac{\sqrt{3}}{2} & -\frac{3}{2} & \frac{\sqrt{3}}{2} & -\frac{1}{2} \end{bmatrix}^{\mathrm{T}}. \tag{6}$$

10
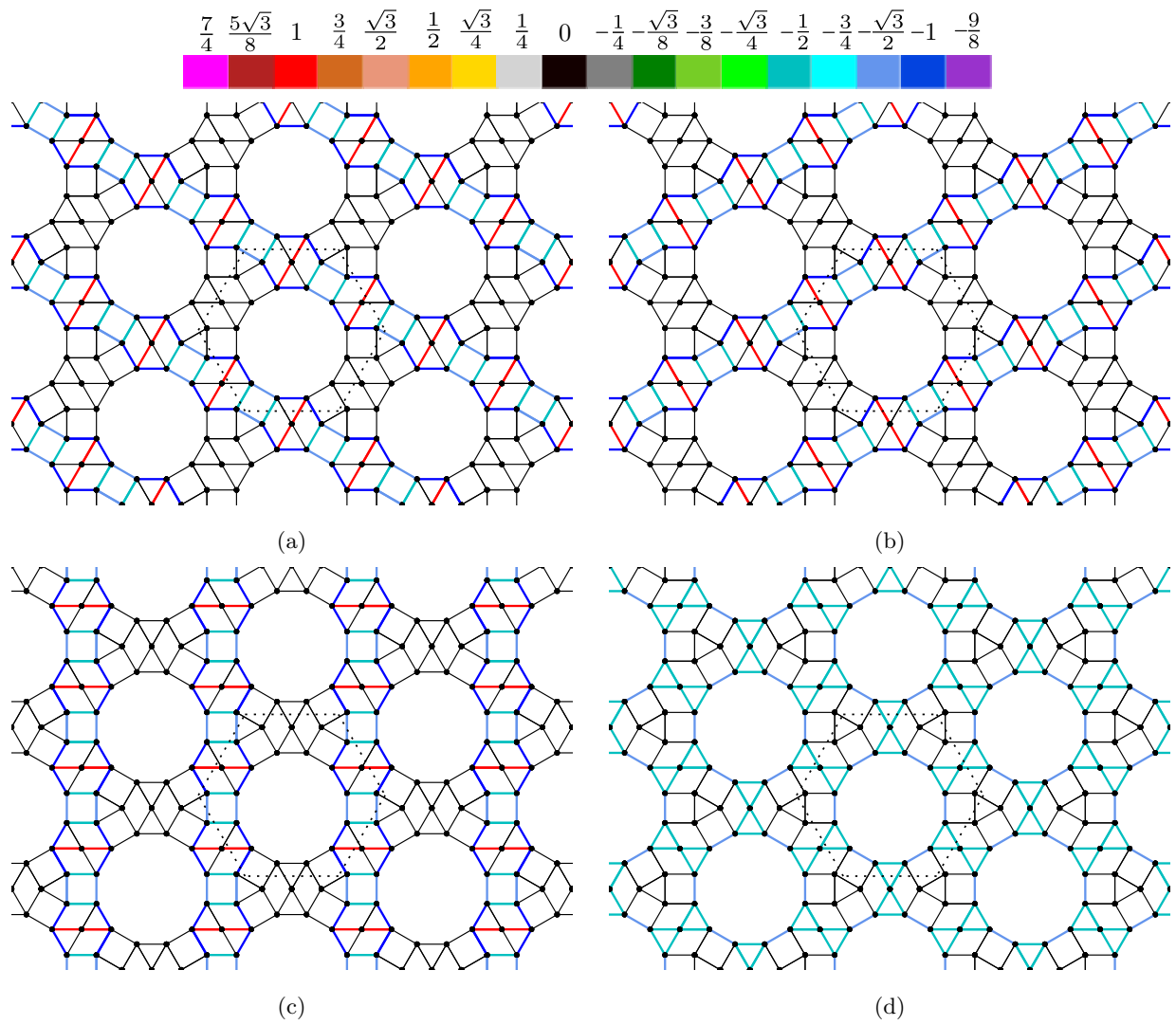
Figure 7: The four linearly independent states of self-stress of the MD micro-architecture. Colours indicate levels of bar tension per the legend shown. (a)-(d) represent column 1-4 of Null(**A**), respectively. The nullspace is given in Appendix.
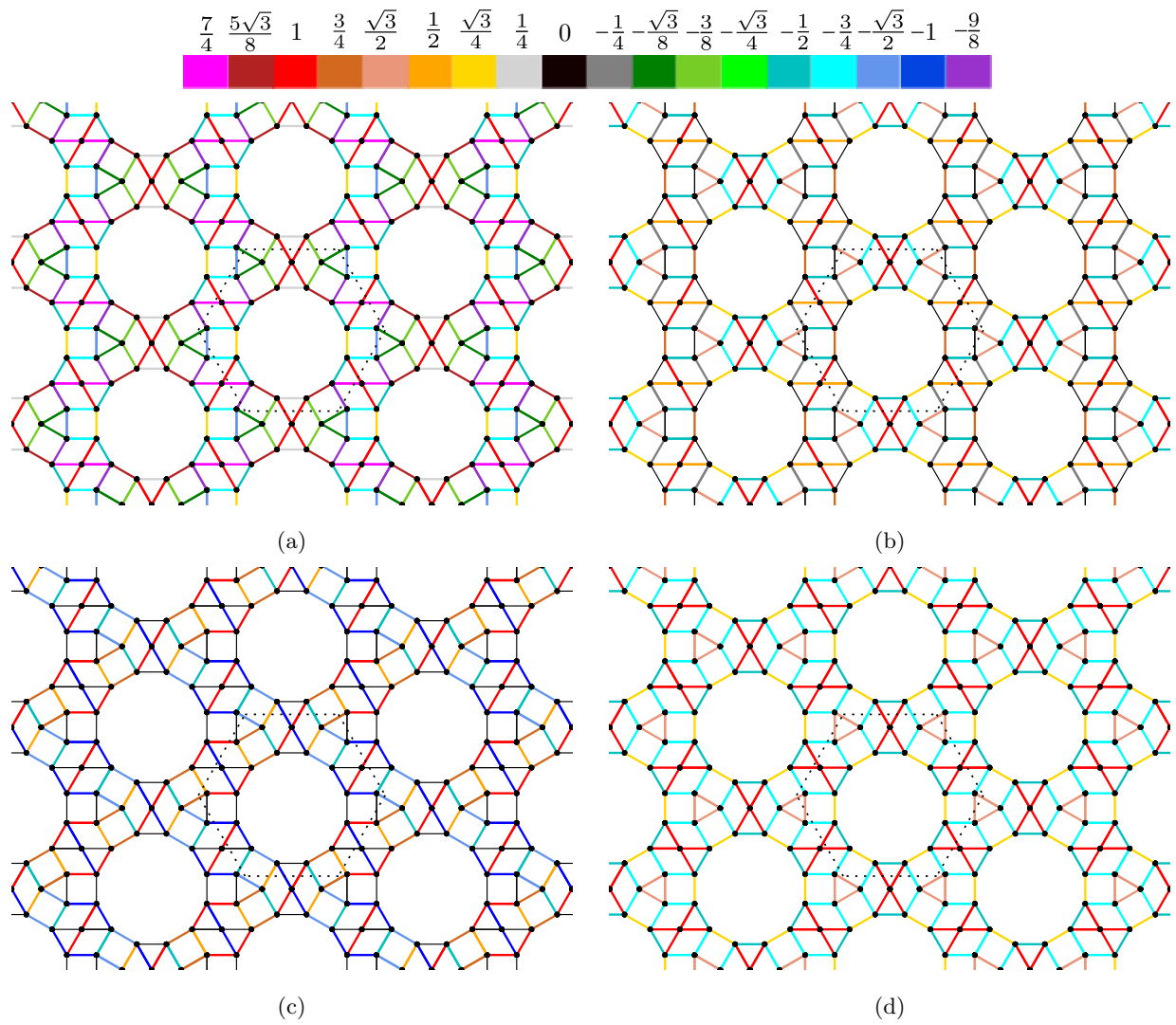
Figure 8: An alternative set of four linearly independent states of self-stress of the MD micro-architecture. Colours indicate levels of bar tension per the legend shown.

12
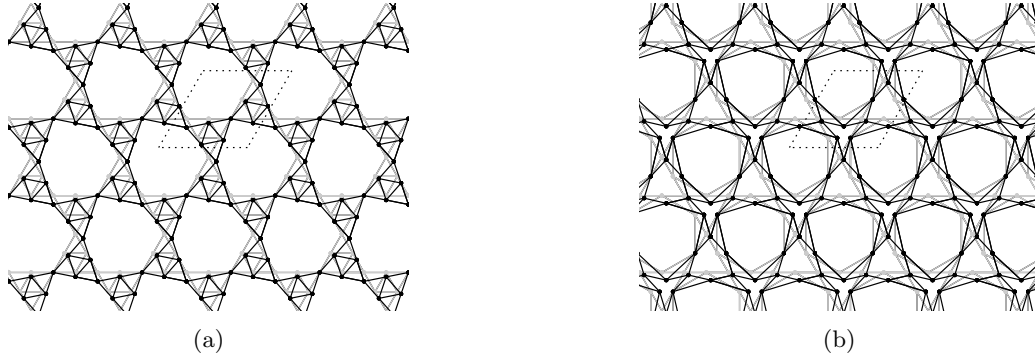
Figure 9: Linearised representations of the unit cell periodic finite mechanisms of the (a) KT and (b) KH micro-architecture. The dotted lines form the outline of a unit cell for both the deformed (shown in black) and undeformed (shown in grey) configuration indicating there is no strain associated with this increment of either of these finite mechanisms.

The first and second columns of null($\mathbf{B}$) represent rigid body translation in the x_2- and x_1-direction, respectively. The third column is a linearised version of a unit cell-periodic finite mechanism, which is depicted in Fig. 9a. It is characterised by opposed rotations by equal amounts around node 6, where two triangles meet. Its linearised version is non strain-producing. The Kagome lattice possesses an analogous unit cell-periodic mechanism, referred to as "internal rigid body rotation" by Pronk et al. (2017).

The KH and KT structures have exactly the same nodal positions, whereas the layout of the connecting members differs, c.f. Figs. 2a and 2b. As in case of the KT structure, null($\mathbf{B}$) of the pin-jointed KH truss (given in Appendix) contains two rigid body displacements and one unit cell-periodic mechanism. The latter is depicted in Fig. 9b. The mechanism of the KH structure clearly differs from that of the KT structure. Still, the linearised version of the KH mechanism is non strain-producing too.

Matrix analysis of the pin-jointed DK truss is performed using the unit cell depicted in Fig. 2c. This unit cell contains 12 nodes, constituting a total of 24 independent displacements, and 24 members allowing for 24 member elongations. This results in a 24×24 compatibility matrix, the nullspace of which reveals *four* non strain-producing periodic mechanisms for this structure, in addition to two rigid-body translations. The periodic mechanisms are illustrated in Fig. 10. The nullspace is given in Appendix.

Finally, the unit cell of the pin-jointed MD truss is depicted in Fig. 2d. It contains 21 nodes and 42 members. The resulting 42×42 compatibility matrix $\mathbf{B}$ is of rank 38; its nullspace (see Appendix) contains four displacement modes that do not result in any member elongation. As for all other considered structures, two of those modes are rigid-body translations. The two remaining linearised mechanisms are shown in Fig. 11. Both mechanisms are non strain-producing.

All of the investigated micro-architectures have only non strain-producing mechanisms. Therefore, none of the mechanisms can be triggered by any 2D macroscopic load. Periodic pin-jointed trusses with these micro-architectures are therefore also found to be rigid from a kinematic point of view, in line with the findings in Section 3.1.

Rigidity was deliberately investigated from a statics point of view first here because of its simplicity. To establish rigidity based on a kinematic analysis, the existence of strain-producing mechanisms must be ruled out. Deformation of the unit cell is not considered in conventional matrix analysis (Pellegrino and Calladine, 1986); mechanisms that distort the unit cell can be determined by using the augmented matrix method, see e.g. Guest and Hutchinson (2003) and Pronk et al. (2017).

4. Elastic properties of the preselected lattice materials

The macroscopic elastic properties of lattice materials with the preselected micro-architectures are determined numerically through finite element (FE) analysis. The Kagome lattice is also analysed for comparison. All calculations are performed with the commercial FE program Abaqus (v6.14). Infinitely large sheets of the 2D lattice materials are modelled using doubly periodic unit cells. Making use of symmetry, it suffices

13
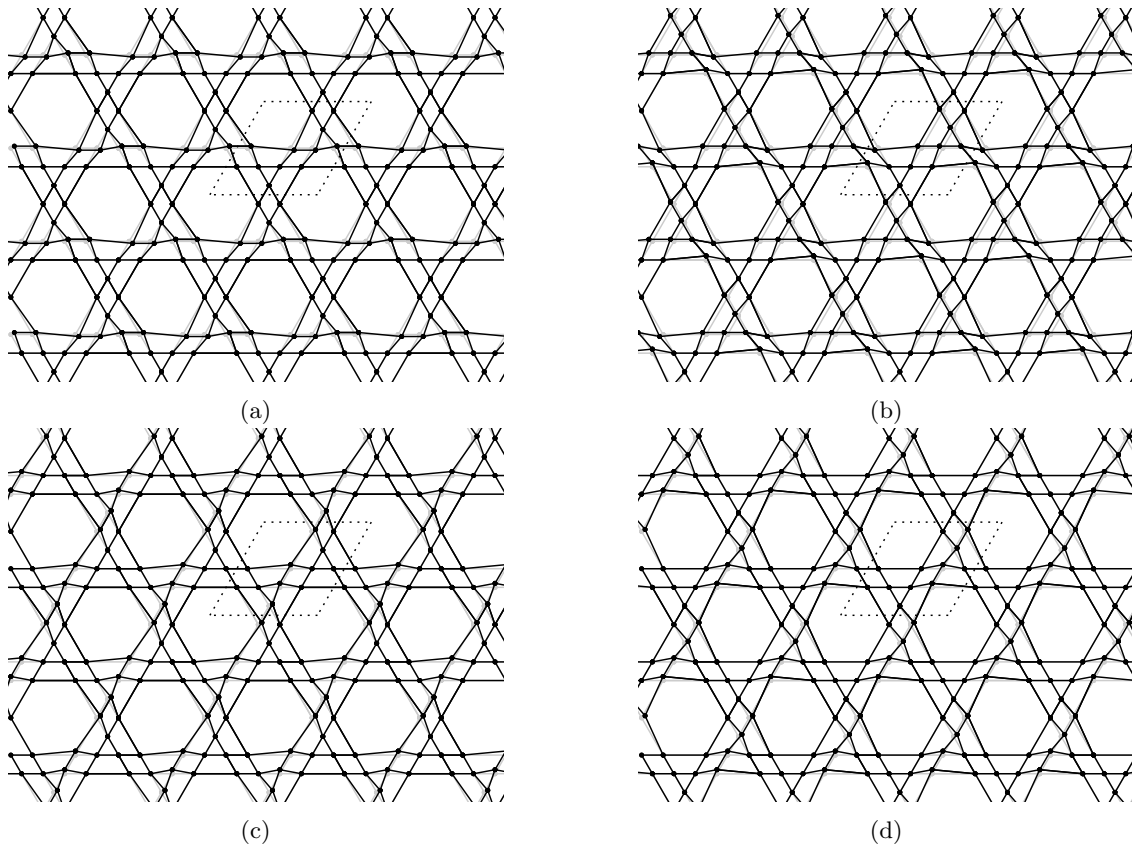
Figure 10: The four non strain-producing linearised unit cell-periodic mechanisms of the DK micro-architecture.
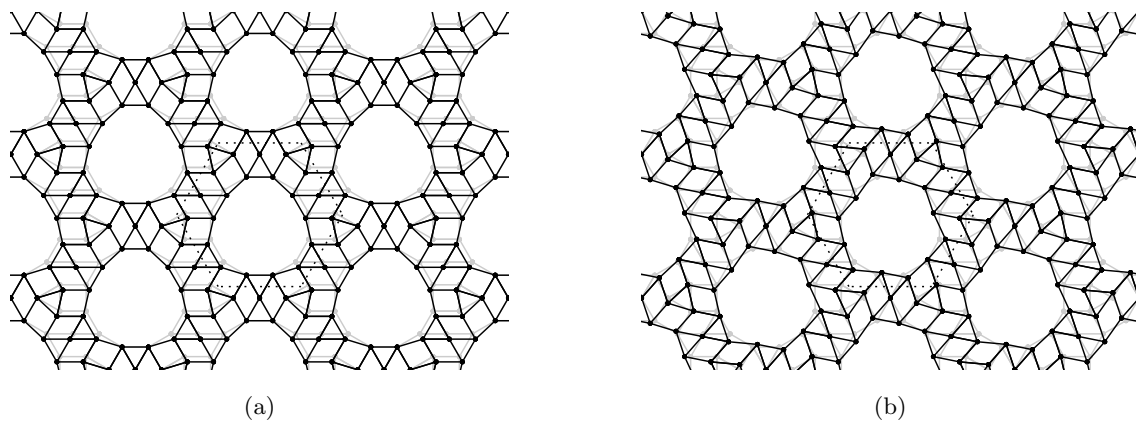
Figure 11: The two non strain-producing linearised unit cell-periodic finite mechanisms of the MD micro-architecture.
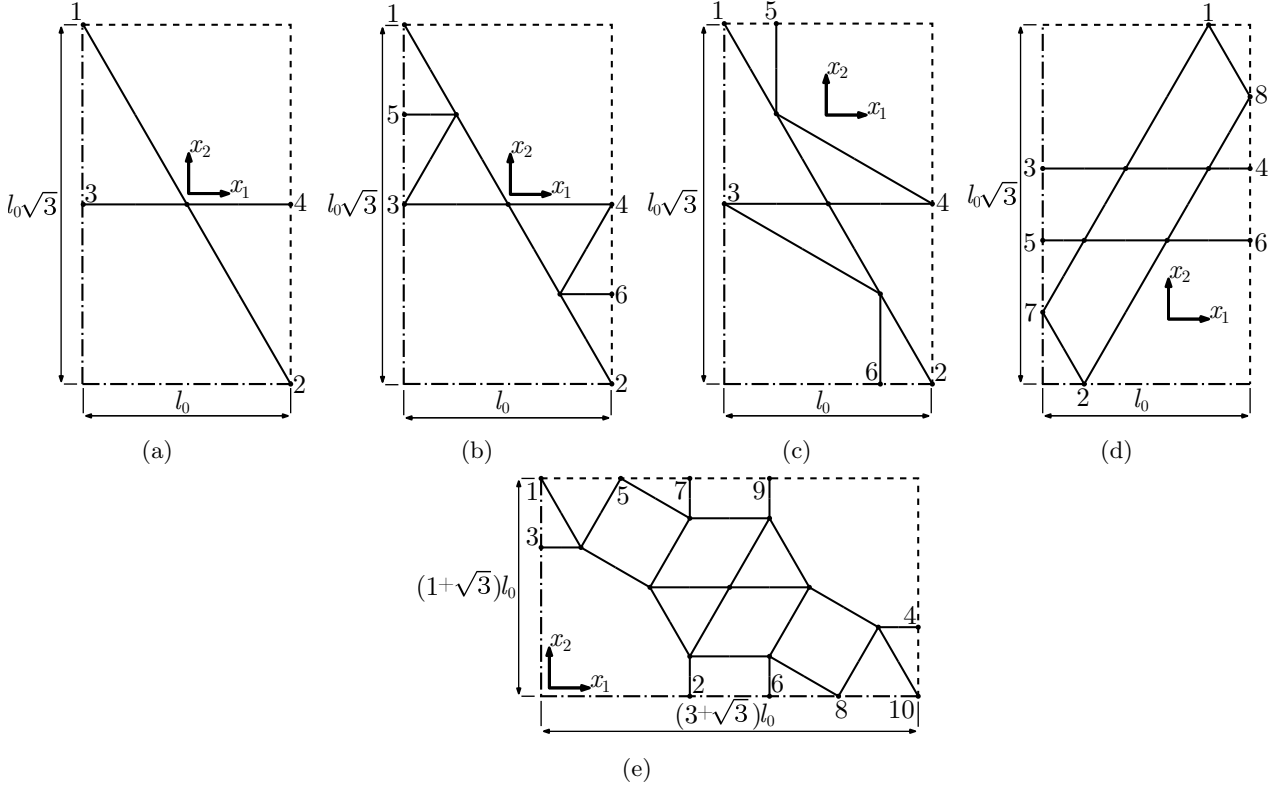
Figure 12: FE geometries for the mechanical characterisation of lattice materials with the (a) Kagome, (b) KT, (c) KH, (d) DK and (e) MD micro-architecture. Dash-dotted symmetry lines used for application of boundary conditions are shown.

to model only one fourth of each of the unit cells as depicted in Fig. 12. The dash-dotted lines in Fig. 12 indicate the axes of symmetry while dashed lines represent unit cell boundaries. Each lattice member is discretised by a single Timoshenko beam element (Abaqus element B22). All beam elements have a rectangular cross-section with in-plane width w and out-of-plane thickness h. The lengths of the struts are at least 10 times greater than the maximum values of w and h. The strut material is linear elastic with Young's modulus E_s and Poisson's ratio ν_s.

Geometrically linear (small strain) uniaxial compression calculations are carried out on the lattice micro-architectures. The dimensions of the quarter unit cells are indicated in Fig. 12. Note that the unit cells in Figs. 12a –12d are identical in size while the unit cell of the MD structure (see Fig. 12e) is much larger.

Loading is applied by imposing displacement boundary conditions. For uniaxial tension/compression in the x_1-direction, the boundary conditions for the Kagome lattice read

$$u_1^{(1)} = u_1^{(3)} = 0, \qquad u_2^{(2)} = 0, \qquad \varphi^{(1)} = \varphi^{(2)} = \varphi^{(3)} = 0, \qquad (7a)$$

$$u_1^{(2)} = u_1^{(4)}, \qquad \varphi^{(4)} = 0, \qquad (7b)$$

$$u_1^{(4)} - u_1^{(3)} = \varepsilon_{11}^* l_0, \qquad (7c)$$

where $u_i^{(J)}$ and $\varphi^{(J)}$ denote the displacement in x_i direction and the in-plane rotation of node J, respectively. The conditions in Eq. (7a) are a direct consequence of symmetry. Those in Eq. (7b) and (7c) enforce periodicity under the applied strain ε_{11}^*. The macroscopic stress resulting from the imposed deformation is given as

$$\sigma_{ij}^* = \frac{1}{A_j} \sum_{k=1}^n f_i^{(k)}, \qquad (8)$$

15

Table 1: Relative densities of the considered structures as a function of in-plane strut width w and mean strut length l.

Structure	Kagome	KT	KH	DK	MD
$\bar{\rho}$	$\sqrt{3}\dfrac{w}{l}$	$\dfrac{3\sqrt{3}}{4}\dfrac{w}{l}$	$\left(\dfrac{7\sqrt{3}}{12}+1\right)\dfrac{w}{l}$	$\sqrt{3}\dfrac{w}{l}$	$\left(7\sqrt{3}-\dfrac{21}{2}\right)\dfrac{w}{l}$

where there are n nodes on the unit cell boundary that has an area A_j normal to the x_j direction. The reaction force in x_i direction on boundary node $k = 1,\dots n$ is denoted with $f_i^{(k)}$. Boundary conditions for the KT, KH, DK and MD structures directly follow the ones given Eqs. (7a) - (7c), and are not given for the sake of brevity.

The effective macroscopic Young's modulus is calculated as

$$E^* = \frac{\sigma_{11}^*}{\varepsilon_{11}^*} \tag{9}$$

while the macroscopic Poisson's ratio is

$$\nu^* = -\frac{\varepsilon_{22}^*}{\varepsilon_{11}^*}. \tag{10}$$

The strain ε_{22}^* is calculated as $\varepsilon_{22}^* = (u_2^{(1)} - u_2^{(2)})/l_0\sqrt{3}$ for the Kagome lattice, for example.

Fig. 13a shows the normalised macroscopic Young's moduli $\bar{E} = E^*/E_s$ for the different micro-architectures as a function of relative density. Expressions for the relative density, i.e. the volume fraction of the solid material are tabulated in Table 1 in terms of the in-plane strut width w and the mean strut length l. Recall that the Kagome, KT and MD micro-architectures have a uniform strut length whereas the KH and DK micro-architectures have members with two different lengths. Therefore, the value of l for the KH and DK structures is determined by taking a weighted average of the lengths of the two types of struts. The density of a structure is varied by changing the in-plane width w only, while the out-of-plane thickness h is kept constant. $\bar{E}$ scales (nearly) linearly with $\bar{\rho}$ for all micro-architectures, indicating stretching-dominated elastic deformation. $\bar{E}$ values calculated for the Kagome lattice are in perfect agreement with those reported by Hyun and Torquato (2002).

The Kagome structure is known to be an ideal micro-architecture in terms of stiffness, i.e. its $\bar{E}$ for a given $\bar{\rho}$ reaches the upper bound for low-density isotropic lattice materials (Hashin and Shtrikman, 1963). Note that the DK structure, having an identical $\bar{E}$ versus $\bar{\rho}$ behaviour, is also a lattice micro-architecture with optimal isotropic stiffness. The KT and KH structures are much more compliant compared to the DK as the concentric triangles and hexagons added to the Kagome structure bear negligible load under uniaxial compression. The MD structure yields the weakest elastic response while the stockiness of its members are comparable with the KT structure. Therefore, it is shown that the micro-architecture is the key determining factor for the elastic response of a lattice material.

Recall that all the structures under investigation are in-plane isotropic. Consequently, two elastic moduli are sufficient to fully capture their elastic properties. Fig. 13b shows the macroscopic Poisson's ratio ν^* of all the micro-architectures as a function of $\bar{\rho}$. The macroscopic Poisson's ratio is higher for the MD structure than for the other structures. The KT, KH and DK lattices have macroscopic Poisson's ratios close to $\nu^* = \frac{1}{3}$, i.e. to the analytical result for a periodic Kagome lattice (Wang and McDowell, 2004). Although the KH and MD lattices are stretching-dominated materials, the struts in them also bend under uni-axial compression, which leads to a slight decrease in ν^* with increasing $\bar{\rho}$.

5. Actuation properties of the preselected lattice materials

Wicks and Guest (2004) quantified the resistance of a lattice material to actuation by calculating the energy consumed by a single actuator replacing a regular member in the micro-architecture. For an actuator that works through an actuation strain ε_{a}, the actuation energy reads

$$W = -\frac{1}{2}t\lambda\varepsilon_{\mathrm{a}}, \tag{11}$$

16
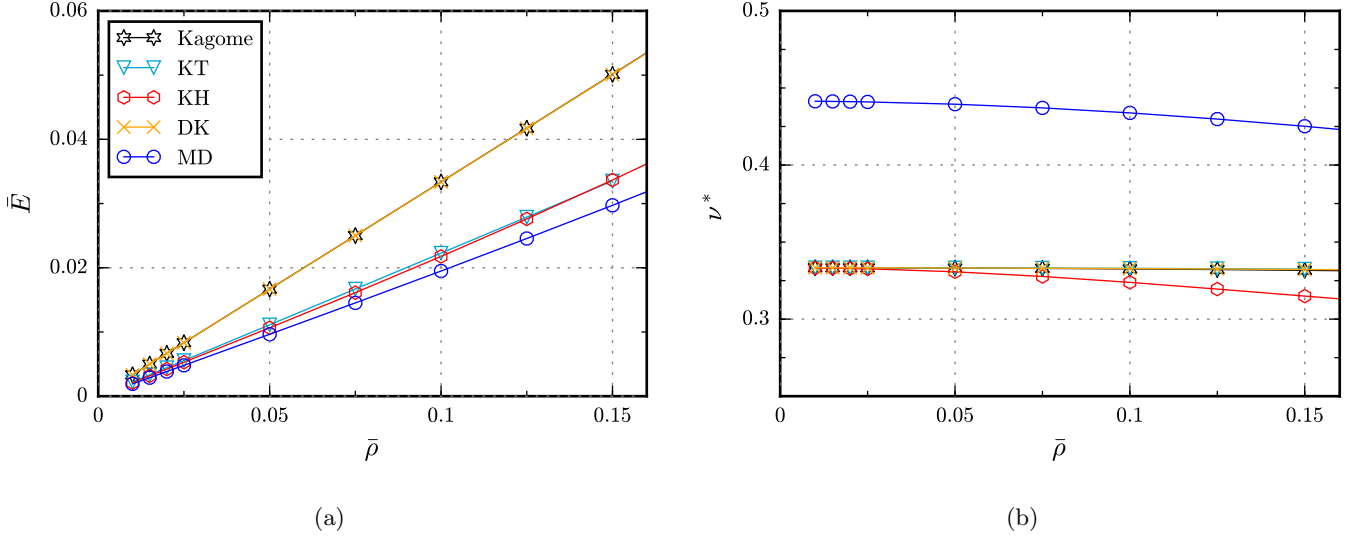
Figure 13: (a) Normalised Young's modulus $\bar{E} = E^*/E_s$ and (b) macroscopic Poisson's ratio of the investigated structures as a function of relative density.

where t is the tension in the actuator beam after actuation is complete, and λ is the original member length. An actuator is assumed to have the same cross-section and material properties as a regular member. A reference energy W_0 is defined as the work done by an actuator if it were surrounded by a fully rigid structure; the tension in the member after actuation would be $t_0 = -E_\mathrm{s}A\varepsilon_\mathrm{a}$, resulting in

$$W_0 = \frac{1}{2}E_\mathrm{s}A\lambda\varepsilon_\mathrm{a}^2, \tag{12}$$

where A is the cross-sectional area of the actuator. The normalised actuation energy is defined as $\hat{W} = W/W_0$; a low value of $\hat{W}$ indicates an easily actuated lattice micro-architecture.

Actuation energies for the preselected structures are calculated using FE models similar to those used in Wicks and Guest (2004) and Pronk et al. (2017). Sheets of lattice material of approximately $800l_0 \times 30l_0\sqrt{3}$ are considered. The large size limits boundary effects on the determined $\hat{W}$. Single member actuation is mimicked by deleting a member at the center and prescribing displacements on the two joints it was connected to, as illustrated in Fig. 14. If required for symmetric actuation, two actuators are placed. The lattice members are discretised by Euler-Bernoulli beam elements (Abaqus element B23) with rectangular cross-sections. $\hat{W}$ values are found to be nearly identical when traction free boundary conditions are replaced with fully clamped conditions on all boundary nodes. The latter (upper bound) results are reported here. Fig. 15a shows the normalised actuation energy $\hat{W}$ for the structures of interest as a function of $\bar{\rho}$. Energy required for actuation can be partitioned into the energy associated with bending W_b, and the energy associated with axial stretching W_s of the beams. Fig. 15b shows W_s/W, i.e. the fraction of W that goes up in stretching the members of the lattice material.

Note that because of its high level of symmetry, actuation of any member of the Kagome micro-architecture is equivalent. The other micro-architectures contain members that are not identical; two kinds of members appear in the KT and KH lattices, three in the DK lattice and there are five different kinds of struts in the MD micro-architecture. Replaced by an actuator, each kind of strut constitutes a different mode of actuation. The most compliant mode was selected for each of the preselected structures. Those are illustrated in Fig. 14.

It is interesting to see that all the considered lattice architectures except for the KH structure result in similarly low values of $\hat{W}$. The high actuation energy of the KH structure seems to be the logical result of the predominantly stretching nature of the deformation during actuation; see Fig. 15b. Surprisingly, at low

17
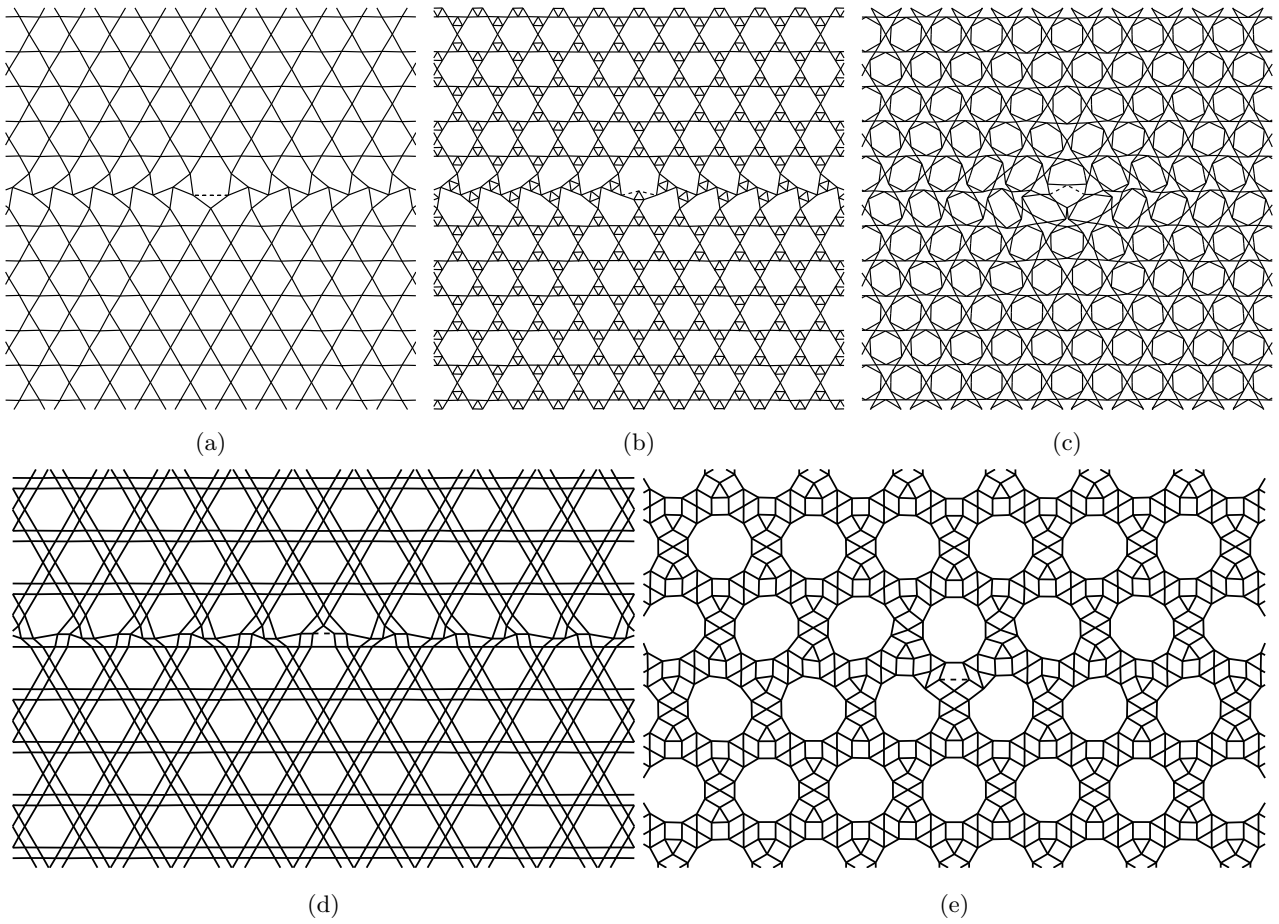
Figure 14: Center portions of five lattices after 'single member' actuation. (a) Kagome, (b) KT, (c) KH, (d) DK and (e) MD. Two members are actuated in the KT and KH lattices to achieve symmetric deformation. Displacements are greatly magnified, $\bar{\rho} = 0.01$.
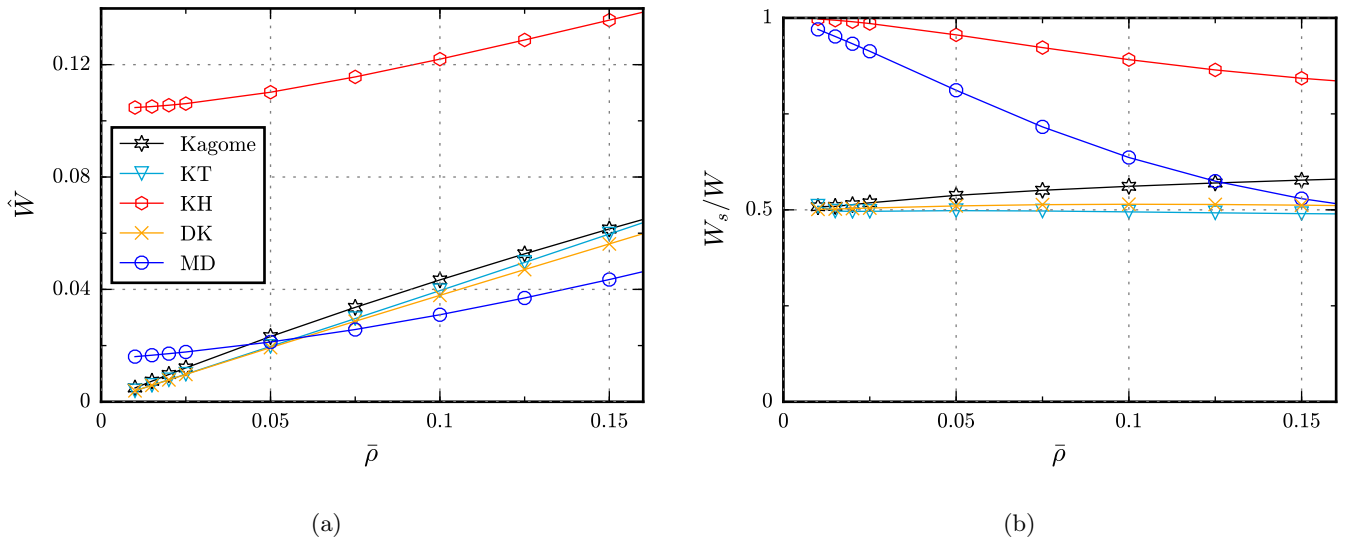
Figure 15: Upper bound for (a) the normalised actuation energy $\hat{W} = W/W_0$ and (b) the fraction of the actuation energy that goes up in axial stretching of members W_s/W.

values of $\bar{\rho}$, the MD structure has a low actuation energy even though almost all of the energy is stored by stretching of members. This implies that only a limited number of struts are deformed due to the lengthening of the actuator and/or that the deformations are very small.

Energy cost of actuation is not the only criterion for the selection of an actuation material. Wicks and Guest (2004) noted that in a Kagome lattice "the distance over which deformation dies away depends on the stockiness". The fact that the deformations are stockiness-dependent, and thus dependent on $\bar{\rho}$, actually explains the approximately linear dependency of $\hat{W}$ on $\bar{\rho}$.

Fig. 14 shows that actuation effects differ greatly between lattice micro-architectures. The Kagome and the KT lattices show very similar responses to actuation; lengthening of the actuator(s) is accommodated by alternating rotations of triangles. In the deformed DK lattice in Fig. 14d, similar rotations of triangles appear, but here only a single row of triangles is involved. Also, the triangles are not directly connected, requiring the displacements to be 'passed along' by deformation of the rhombi and trapeziums in between. In the actuated MD lattice in Fig. 14e, the affected 'corridor' is wider. Here too, rotations of triangles and deformation of rhombi are apparent. The effects of actuation are very localised in the KH lattice as shown in Fig. 14c. The structure is severely distorted in the direct vicinity of the actuator, but within a distance of a few unit cells the effects diminish.

Fig. 16a shows the attenuation distances plotted against $\bar{\rho}$ for all the micro-architectures. Considering members aligned with the actuator, attenuation distance is defined as the distance from the actuator at which the deformations, in the direction of actuation, have reduced to 20% of the displacement of the tip(s) of the actuator. Naturally, the attenuation distance l_a decreases with increasing density for all structures. Figure 16b shows exactly how the displacements attenuate with distance (to the right of the actuator) for $\bar{\rho} = 0.01$.

It is interesting to see that a low(er) actuation energy is not necessarily associated with a large(r) attenuation distance. Compare for instance the results of the Kagome, KT and DK structures. Still, deformations are limited to a very small region surrounding the actuator in the KH lattice, which has the highest actuation energy. The MD lattice shows a very different attenuation behaviour than the other structures: after a large reduction ($\sim 60\%$) of the displacement magnitude within a small distance from the actuator, the deformations attenuate very gradually.

19
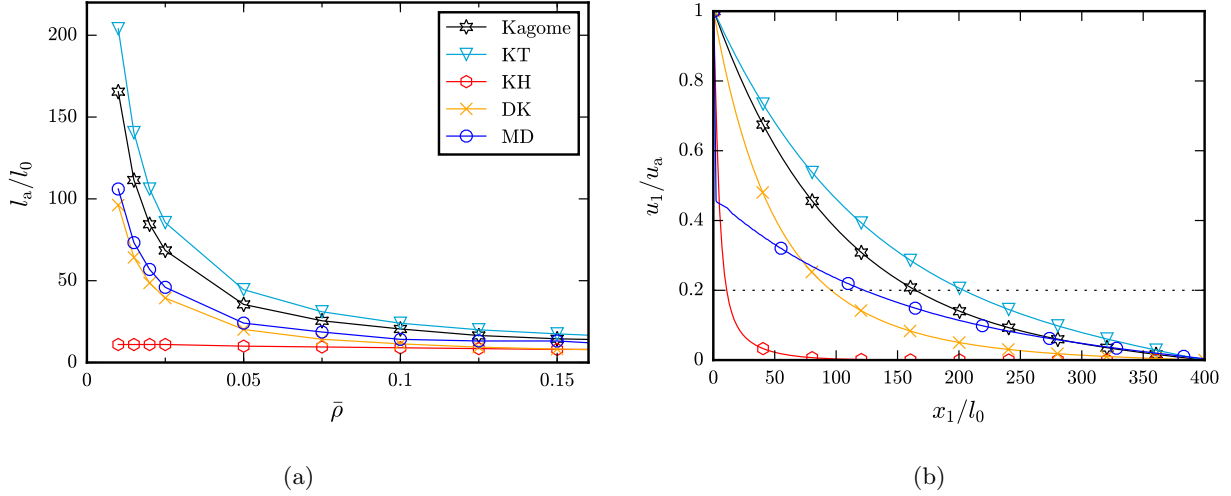
Figure 16: (a) Normalised attenuation distance l_a/l_0 as a function of relative density; the distance, measured in line with the actuator, at which the displacements have damped out to 20% of the displacement of the actuator's tip(s). l_0 is defined in Fig. 12. (b) Decay of displacements/deformations (in the direction of actuation) with distance from the actuator for $\bar{\rho} = 0.01$. Not all data points are marked to increase clarity. The dotted line indicates the 20%-displacement level of Fig. 16a.

6. Discussion

All the findings of his study are summarised in Table 2. Since all of the preselected micro-architectures satisfy the Maxwell condition given in Eq. (3), $s = m$; the number of states of self stress is equal to the number of inextensional displacement modes. Moreover, (linear combinations of) the states of self-stress associated with each of the micro-architectures can be linked to each of the macroscopic stresses that exist in 2D; $S = 3$. That is, all the micro-architectures considered are rigid when pin-jointed. This rules out the existence of strain-producing mechanisms; $ms = 0$. Table 2 includes the static/kinematic properties of the repetitive Kagome, Hexagonal Cupola and Triangulated micro-architectures, which were gathered from literature (Wicks and Guest, 2004; Hutchinson and Fleck, 2006; Pronk et al., 2017). Note that the Kagome and Hexagonal Cupola trusses both satisfy the Maxwell condition whereas $s > m$ for the Triangulated structure.

Matrix analysis of periodic trusses with the KH and KT micro-architectures showed they have similar static and kinematic properties. In fact, their entries in Table 2 are identical to the values for the Kagome structure. In Section 4, lattices with the KH and KT structure were shown to perform very similarly in terms of macroscopic elastic properties. On the contrary, their actuation performances could not be further apart. Firstly, Fig. 15a shows that a KH lattice requires by far the highest actuation energy of all the preselected structures, while the KT structure is amongst the lowest. Secondly, in terms of attenuation the KT and KH structures actually set the extremes (Fig. 16): deformation hardly spreads away from an actuator in a KH lattice, while it damps out the slowest in KT lattice material.

For the range of $\bar{\rho}$ considered, Fig. 15a shows that a DK lattice material requires a lower amount of energy for actuation than a Kagome lattice. Also, as shown in Figure 13a, the two lattices have equal macroscopic stiffness values at equal values of $\bar{\rho}$. Therefore, the DK lattice outperforms the Kagome lattice, albeit actuation induced deformations do attenuate more quickly in a DK lattice according to Fig. 16. However, the latter is not independent of scale (in contrast to the normalised actuation energy): if a Kagome and a DK lattice of the same density $\bar{\rho}$ are constructed out of beams of identical in-plane width w, the unit cell dimensions of the DK lattice are twice as large as those of the Kagome lattice. In this case, the attenuation distance is larger in the DK lattice.

Periodic pin-jointed trusses with the DK and MD micro-architecture have $s = 6$ and $s = 4$, respectively, which implies these structures are statically indeterminate. Therefore, the actuation energy values found for

20

Table 2: Properties of periodic trusses/rigid-jointed lattices with seven different micro-architectures.

Property	Micro-architecture(s)				
	Kagome KT KH	DK	MD	Triangulated	Hex. Cupola
s (Linearly independent states of self-stress)	3	6	4	6	3
S (Supported linearly independent macroscopic stress states)	3	3	3	3	1
m (Linearly independent inextensional displacement modes)	3	6	4	2	3
ms (Linearly independent strain-producing mechanisms)	0	0	0	0	2
Deformation behaviour	Stretching-dominated	Stretching-dominated	Stretching-dominated	Stretching-dominated	Bending-dominated
Actuation energy scaling	$\hat{W} \propto \bar{\rho}^1$	$\hat{W} \propto \bar{\rho}^1$	$\hat{W} \propto \bar{\rho}^1$	$\hat{W} \propto \bar{\rho}^0$	$\hat{W} \propto \bar{\rho}^2$

the DK and MD lattices are surprisingly low. However, it is the presence of non strain-producing mechanisms that facilitates easy actuation for the DK and MD lattices. The triangulated lattice is another well-known lattice which is statically indeterminate. Wicks and Guest (2004) found that it has a high actuation energy, independent of the value of $\bar{\rho}$. The key difference is that, a repetitive triangulated truss with $s = 6$ and $m = 2$ has no mechanism, which means that actuation-induced deformation in a triangulated lattice results in strut stretching almost exclusively. In light of these findings, the set of topological criteria to be satisfied for the suitability of a lattice micro-architecture for actuation can be refined. For an isotropic 2D lattice material to be suitable for actuation, its pin-jointed version:

i) must satisfy Maxwell's stability criterion,

ii) must be able to sustain any state of planar macroscopic stress, i.e. $S = 3$.

The second criterion directly implies that the pin-jointed version of the lattice material has *non strain-producing* mechanism(s) only.

7. Conclusion

The lattice micro-architectures presented in this paper allow for the following conclusions to be drawn. First, there are structures that can compete with the Kagome architecture in terms of suitability for actuation. Currently, the DK structure is the only serious competitor, but the other proposed designs too constitute 2D-isotropic stretching-dominated lattices, and all except one result in similar (low) actuation energies. Secondly, a lattice material with a statically indeterminate structure does not necessarily have a high actuation energy. Such a structure does not always result in $\hat{W} \propto \bar{\rho}^0$ either. Finally, the current set of topological criteria for the suitability of a lattice micro-architecture for actuation does not guarantee a low actuation energy for the corresponding rigid-jointed lattice material. The KH lattice demonstrates the latter.

Appendix - Nullspaces

KT:

$$\text{null}(\boldsymbol{A}) = \begin{bmatrix} 1 & 0 & 0 & 1 & 0 & 0 & 0 & 0 & 0 & 0 & 0 & 1 & 0 & 0 & 1 & 0 & 0 \\ 0 & 1 & 0 & 0 & 0 & 0 & 0 & 0 & 0 & 1 & 0 & 0 & 0 & 0 & 1 & 0 & 1 & 0 \\ 0 & 0 & 0 & 0 & 0 & 0 & 1 & 1 & 1 & 0 & 0 & 0 & 0 & 0 & 0 & 0 & 0 & 1 \end{bmatrix}^{\mathrm{T}} \tag{A-1}$$

$$\text{null}(\boldsymbol{B}) = \begin{bmatrix} 0 & 1 & 0 & 1 & 0 & 1 & 0 & 1 & 0 & 1 & 0 & 1 & 0 & 1 & 0 & 1 & 0 & 1 \\ 1 & 0 & 1 & 0 & 1 & 0 & 1 & 0 & 1 & 0 & 1 & 0 & 1 & 0 & 1 & 0 & 1 & 0 \\ \sqrt{3} & -1 & \frac{\sqrt{3}}{2} & -\frac{1}{2} & \frac{\sqrt{3}}{2} & -\frac{3}{2} & 0 & -2 & 0 & -1 & 0 & 0 & 0 & -1 & \frac{\sqrt{3}}{2} & -\frac{3}{2} & \frac{\sqrt{3}}{2} & -\frac{1}{2} \end{bmatrix}^{\mathrm{T}} \tag{A-2}$$

KH:

$$\text{null}(\boldsymbol{A}) = \begin{bmatrix} 1 & 0 & 0 & 1 & 0 & 0 & 0 & 0 & 1 & 0 & 0 & 0 & 1 & 0 & 0 & 0 & 0 & 0 \\ 0 & 1 & 0 & 0 & 0 & 0 & 0 & 1 & 0 & 0 & 0 & 1 & 0 & 0 & 0 & 1 & 0 & 0 \\ 0 & 0 & 0 & 0 & 1 & 1 & 1 & 0 & 0 & 0 & 0 & 0 & 0 & 0 & 0 & 0 & 1 & 0 \end{bmatrix}^{\mathrm{T}} \tag{A-3}$$

$$\text{null}(\boldsymbol{B}) = \begin{bmatrix} \frac{1}{2} & -\frac{\sqrt{3}}{6} & 0 & 0 & 1 & 0 & \frac{1}{2} & -\frac{\sqrt{3}}{6} & \frac{1}{2} & -\frac{\sqrt{3}}{2} & \frac{1}{2} & -\frac{\sqrt{3}}{6} & \frac{1}{2} & -\frac{\sqrt{3}}{2} & 1 & 0 & 0 & 0 \\ 1 & 0 & 1 & 0 & 1 & 0 & 1 & 0 & 1 & 0 & 1 & 0 & 1 & 0 & 1 & 0 & 1 & 0 \\ 0 & 1 & 0 & 1 & 0 & 1 & 0 & 1 & 0 & 1 & 0 & 1 & 0 & 1 & 0 & 1 & 0 & 1 \end{bmatrix}^{\mathrm{T}} \tag{A-4}$$

DK:

$$\text{null}(\boldsymbol{A}) = \begin{bmatrix} 1 & 0 & 0 & 0 & 0 & 0 & 0 & 0 & 1 & 0 & 0 & 0 & 0 & 0 & 1 & 0 & 1 & 0 & 0 & 0 & 0 & 0 & 0 \\ 0 & 0 & 1 & 1 & 0 & 0 & 0 & 0 & 0 & 0 & 1 & 0 & 0 & 0 & 0 & 0 & 0 & 0 & 0 & 1 & 0 & 0 & 0 \\ 0 & 0 & 0 & 0 & 0 & 0 & 0 & 0 & 1 & 0 & 0 & 0 & 0 & 0 & 1 & 0 & 0 & 0 & 1 & 0 & 1 & 0 & 0 \\ 0 & 0 & 0 & 0 & 0 & 1 & 1 & 1 & 0 & 0 & 0 & 0 & 0 & 0 & 0 & 0 & 0 & 0 & 0 & 0 & 0 & 1 & 0 \\ 0 & 1 & 0 & 0 & 1 & 0 & 0 & 0 & 0 & 0 & 0 & 0 & 0 & 0 & 0 & 1 & 0 & 0 & 0 & 0 & 0 & 1 & 0 \\ 0 & 0 & 0 & 0 & 0 & 0 & 0 & 0 & 0 & 0 & 1 & 1 & 1 & 0 & 0 & 0 & 0 & 0 & 0 & 0 & 0 & 0 & 1 \end{bmatrix}^{\mathrm{T}} \tag{A-5}$$

$$\text{null}(\boldsymbol{B}) = \begin{bmatrix} 0 & 0 & 0 & 0 & 0 & 0 & \frac{\sqrt{3}}{2} & \frac{1}{2} & \frac{\sqrt{3}}{2} & -\frac{1}{2} & \frac{\sqrt{3}}{2} & -\frac{1}{2} & \frac{\sqrt{3}}{2} & \frac{1}{2} & 0 & 0 & 0 & 0 & 0 & 0 & 0 & 0 & 0 & 0 \\ -\frac{\sqrt{3}}{2} & \frac{1}{2} & 0 & 0 & -\frac{\sqrt{3}}{2} & \frac{1}{2} & 0 & 0 & 0 & 0 & 0 & 0 & 0 & 0 & 1 & 0 & 1 & 0 & 0 & 0 & 0 & 0 & 0 & 0 \\ \frac{\sqrt{3}}{2} & \frac{1}{2} & 0 & 0 & 0 & 0 & 0 & 0 & 0 & 1 & 0 & 0 & 0 & 0 & 0 & 0 & 0 & 0 & 1 & 0 & 0 & \frac{\sqrt{3}}{2} & \frac{1}{2} \\ 0 & 0 & \frac{\sqrt{3}}{2} & \frac{1}{2} & \frac{\sqrt{3}}{2} & \frac{1}{2} & 0 & 0 & 0 & 0 & 1 & 0 & 0 & 0 & 0 & 0 & 0 & 0 & 0 & 0 & 1 & 0 & 0 \\ 0 & 1 & 0 & 1 & 0 & 1 & 0 & 1 & 0 & 1 & 0 & 1 & 0 & 1 & 0 & 1 & 0 & 1 & 0 & 1 & 0 & 1 & 0 & 1 \\ 1 & 0 & 1 & 0 & 1 & 0 & 1 & 0 & 1 & 0 & 1 & 0 & 1 & 0 & 1 & 0 & 1 & 0 & 1 & 0 & 1 & 0 & 1 & 0 \end{bmatrix}^{\mathrm{T}} \tag{A-6}$$

22

493 MD:

$$
\text{null}(\boldsymbol{A}) =
\begin{bmatrix}
0 & -\frac{\sqrt{3}}{2} & 0 & 0 \\
-1 & -\frac{1}{2} & 0 & 0 \\
1 & 0 & 0 & -\frac{1}{2} \\
0 & 1 & 0 & -\frac{1}{2} \\
-\frac{\sqrt{3}}{2} & 0 & 0 & 0 \\
-\frac{1}{2} & -1 & 0 & 0 \\
0 & -\frac{1}{2} & -1 & 0 \\
-\frac{1}{2} & 0 & -1 & 0 \\
-1 & -1 & 0 & -\frac{1}{2} \\
0 & -\frac{\sqrt{3}}{2} & 0 & -\frac{\sqrt{3}}{2} \\
-\frac{\sqrt{3}}{2} & 0 & 0 & -\frac{\sqrt{3}}{2} \\
0 & 0 & 1 & -\frac{1}{2} \\
0 & 1 & 0 & -\frac{1}{2} \\
0 & -1 & -1 & -\frac{1}{2} \\
0 & 0 & 1 & -\frac{1}{2} \\
-1 & 0 & -1 & -\frac{1}{2} \\
1 & 0 & 0 & -\frac{1}{2} \\
0 & -1 & -\frac{1}{2} & 0 \\
0 & 0 & -\frac{\sqrt{3}}{2} & -\frac{\sqrt{3}}{2} \\
-1 & 0 & -\frac{1}{2} & 0 \\
0 & 0 & -\frac{\sqrt{3}}{2} & -\frac{\sqrt{3}}{2} \\
-1 & 0 & -1 & -\frac{1}{2} \\
0 & -1 & -1 & -\frac{1}{2} \\
-\frac{\sqrt{3}}{2} & 0 & 0 & -\frac{\sqrt{3}}{2} \\
0 & -\frac{\sqrt{3}}{2} & 0 & -\frac{\sqrt{3}}{2} \\
-1 & -1 & 0 & -\frac{1}{2} \\
-\frac{1}{2} & -1 & 0 & 0 \\
0 & 1 & 0 & -\frac{1}{2} \\
1 & 0 & 0 & -\frac{1}{2} \\
-1 & -\frac{1}{2} & 0 & 0 \\
0 & -\frac{\sqrt{3}}{2} & 0 & 0 \\
0 & 0 & -\frac{\sqrt{3}}{2} & 0 \\
-1 & 0 & -\frac{1}{2} & 0 \\
1 & 0 & 0 & -\frac{1}{2} \\
0 & 0 & 1 & -\frac{1}{2} \\
-\frac{1}{2} & 0 & -1 & 0 \\
-\frac{\sqrt{3}}{2} & 0 & 0 & 0 \\
0 & 0 & -\frac{\sqrt{3}}{2} & 0 \\
0 & -1 & -\frac{1}{2} & 0 \\
0 & 1 & 0 & -\frac{1}{2} \\
0 & 0 & 1 & -\frac{1}{2} \\
0 & -\frac{1}{2} & -1 & 0
\end{bmatrix},
\quad
\text{null}(\boldsymbol{B}) =
\begin{bmatrix}
0 & 0 & 1 & 0 \\
0 & 1 & 0 & -1 \\
0 & 0 & 1 & 0 \\
0 & 1 & 0 & 0 \\
0 & 0 & 1 & 0 \\
0 & 1 & 0 & 1 \\
-\frac{\sqrt{3}}{3} & 0 & 1 & -\frac{2\sqrt{3}}{3} \\
1 & 1 & 0 & 1 \\
\frac{\sqrt{3}}{3} & 0 & 1 & -\frac{\sqrt{3}}{3} \\
1 & 1 & 0 & 0 \\
0 & 0 & 1 & \frac{\sqrt{3}}{2} \\
0 & 1 & 0 & -\frac{1}{2} \\
0 & 0 & 1 & \frac{\sqrt{3}}{2} \\
0 & 1 & 0 & \frac{1}{2} \\
-\frac{\sqrt{3}}{3} & 0 & 1 & -\frac{\sqrt{3}}{6} \\
1 & 1 & 0 & \frac{1}{2} \\
-\frac{\sqrt{3}}{3} & 0 & 1 & -\frac{\sqrt{3}}{6} \\
1 & 1 & 0 & \frac{3}{2} \\
\frac{\sqrt{3}}{3} & 0 & 1 & \frac{\sqrt{3}}{6} \\
1 & 1 & 0 & -\frac{1}{2} \\
\frac{\sqrt{3}}{3} & 0 & 1 & \frac{\sqrt{3}}{6} \\
1 & 1 & 0 & \frac{1}{2} \\
-\frac{\sqrt{3}}{3} & 0 & 1 & \frac{\sqrt{3}}{3} \\
1 & 1 & 0 & 0 \\
-\frac{\sqrt{3}}{3} & 0 & 1 & \frac{\sqrt{3}}{3} \\
1 & 1 & 0 & 1 \\
\frac{\sqrt{3}}{3} & 0 & 1 & \frac{2\sqrt{3}}{3} \\
1 & 1 & 0 & 0 \\
\frac{\sqrt{3}}{3} & 0 & 1 & \frac{2\sqrt{3}}{3} \\
1 & 1 & 0 & 1 \\
\frac{\sqrt{3}}{3} & 0 & 1 & -\frac{\sqrt{3}}{3} \\
1 & 1 & 0 & 1 \\
-\frac{\sqrt{3}}{3} & 0 & 1 & -\frac{2\sqrt{3}}{3} \\
1 & 1 & 0 & 0 \\
\frac{\sqrt{3}}{3} & 0 & 1 & \frac{\sqrt{3}}{6} \\
1 & 1 & 0 & \frac{3}{2} \\
-\frac{\sqrt{3}}{3} & 0 & 1 & -\frac{\sqrt{3}}{6} \\
1 & 1 & 0 & -\frac{1}{2} \\
0 & 0 & 1 & -\frac{\sqrt{3}}{2} \\
0 & 1 & 0 & -\frac{1}{2} \\
0 & 0 & 1 & -\frac{\sqrt{3}}{2} \\
0 & 1 & 0 & \frac{1}{2}
\end{bmatrix}
\tag{A-7}
$$

References

494 Ashby, M. F., Evans, A. G., Fleck, N. A., Gibson, L. J., Hutchinson, J. W., Wadley, H. N. G., 2000. Metal Foams: A Design Guide. Butterworth-Heinemann, Oxford.

497 Ayas, C., Tekoğlu, C., 2018. On the sufficient symmetry conditions for isotropy of elastic moduli. Journal of Applied Mechanics 85 (074502), 1 – 5.

Critchlow, K., 1970. Order in Space: A Design Source Book. Viking Press.

Deshpande, V. S., Ashby, M. F., Fleck, N. A., 2001. Foam topology: Bending versus stretching dominated architectures. Acta Materialia 49 (6), 1035 – 1040.

Donev, A., Torquato, S., 2003. Energy-efficient actuation in infinite lattice structures. Journal of the Mechanics and Physics of Solids 51 (8), 1459 – 1475.

dos Santos e Lucato, S. L., McMeeking, R. M., Evans, A. G., 2005. Actuator placement optimization in a kagome based high authority shape morphing structure. Smart Materials and Structures 14 (4), 869– 875.

dos Santos e Lucato, S. L., Wang, J., Maxwell, P., McMeeking, R. M., Evans, A. G., 2004. Design and demonstration of a high authority shape morphing structure. International Journal of Solids and Structures 41 (13), 3521 – 3543.

Fleck, N. A., 2004. An overview of the mechanical properties of foams and periodic lattice materials. In: R.F. Singer, C. Körner, V. Altstädt, H. Münstedt (Eds.). Cellular Metals and Polymers. Vol. 44. Trans Tech Publications.

Gibson, L. J., Ashby, M. F., 1997. Cellular Solids: Structure and Properties, 2nd Edition. Cambridge University Press, Cambridge.

Guest, S. D., Hutchinson, J. W., 2003. On the determinacy of repetitive structures. Journal of the Mechanics and Physics of Solids 51 (3), 383–391.

Hashin, Z., Shtrikman, S., 1963. A variational approach to the theory of the elastic behaviour of multiphase materials. Journal of the Mechanics and Physics of Solids 11, 127–140.

Hutchinson, R. G., Fleck, N. A., 2006. The structural performance of the periodic truss. Journal of the Mechanics and Physics of Solids 54 (4), 756 – 782.

Hutchinson, R. G., Wicks, N., Evans, A. G., Fleck, N. A., Hutchinson, J. W., 2003. Kagome plate structures for actuation. International Journal of Solids and Structures 40 (25), 6969 – 6980.

Hyun, S., Torquato, S., 1 2002. Optimal and Manufacturable Two-dimensional, Kagome-like Cellular Solids. Journal of Materials Research 17, 137–144.

Maxwell, J. C., 1864. On the calculation of the equilibrium and stiffness of frames. Philosophical Magazine 27 (182), 294–299, (Paper XXVI in Collected Papers, Cambridge University Press, 1890).

Onck, P. R., 2002. Cosserat modeling of cellular solids. Comptes Rendus Mécanique 330 (11), 717 – 722.

Pellegrino, S., Calladine, C. R., 1986. Matrix analysis of statically and kinematically indeterminate frameworks. International Journal of Solids and Structures 22 (4), 409 – 428.

Pronk, T., Ayas, C., Tekoğlu, C., 2017. A quest for 2d lattice materials for actuation. Journal of the Mechanics and Physics of Solids 105, 199–216.

Wang, A.-J., McDowell, D., April 2004. In-plane stiffness and yield strength of periodic metal honeycombs. Journal of Engineering Materials and Technology 126, 137 – 156.

Wicks, N., Guest, S. D., 2004. Single member actuation in large repetitive truss structures. International Journal of Solids and Structures 41 (3-4), 965 – 978.

Wicks, N., Hutchinson, J. W., 2004. Sandwich Plates Actuated by a Kagome Planar Truss. Journal of Applied Mechanics 71 (5), 652–662.

24